Journal of Computational and Applied Mathematics 234 (2010) 3283–3302

Contents lists available at ScienceDirect

Journal of Computational and Applied Mathematics

journal homepage: www.elsevier.com/locate/cam

Explicit local time-stepping methods for Maxwell's equations☆

Marcus J. Grote*, Teodora Mitkova

Department of Mathematics, University of Basel, Rheinsprung 21, 4051 Basel, Switzerland

ARTICLE INFO

Article history:
Received 8 September 2009
Received in revised form 7 April 2010

MSC:
65N30

Keywords:
Discontinuous Galerkin methods
Electromagnetic waves
Explicit time integration
Finite element methods
Local time-stepping
Maxwell's equations

ABSTRACT

Explicit local time-stepping methods are derived for time dependent Maxwell equations in conducting and non-conducting media. By using smaller time steps precisely where smaller elements in the mesh are located, these methods overcome the bottleneck caused by local mesh refinement in explicit time integrators. When combined with a finite element discretisation in space with an essentially diagonal mass matrix, the resulting discrete time-marching schemes are fully explicit and thus inherently parallel. In a non-conducting source-free medium they also conserve a discrete energy, which provides a rigorous criterion for stability. Starting from the standard leap-frog scheme, local time-stepping methods of arbitrarily high accuracy are derived for non-conducting media. Numerical experiments with a discontinuous Galerkin discretisation in space validate the theory and illustrate the usefulness of the proposed time integration schemes.

1. Introduction

The need to simulate electromagnetic wave phenomena of increasing complexity drives the quest for more general and efficient numerical methods. The first and probably most popular method, the finite difference time domain (FDTD) scheme [1], is simple and efficient on structured (Cartesian) grids, but on oblique or curved boundaries and interfaces it suffers from the inaccurate representation of the solution (staircase approximation) [2]. Moreover, higher order FDTD methods are generally difficult to implement near interfaces and boundaries. In contrast, finite element methods (FEMs) can handle unstructured grids and complex geometry, regardless of the order of approximation. They also provide rigorous a posteriori error estimates which are useful for local adaptivity and error control.

Different finite element discretisations of Maxwell's equations are available, such as edge elements [3–5] and nodal elements [6,7]. Although edge elements may be the most satisfactory from a theoretical point of view [8], in particular near re-entrant corners, they are less attractive for time-dependent computations because the solution of a linear system is required at every time step. Indeed, in the case of triangular or tetrahedral edge elements, the entries of the diagonal matrix resulting from mass-lumping are not necessarily strictly positive [9]. Therefore, explicit time-stepping cannot be used in general. In contrast, standard (H^1-conforming) nodal elements naturally lead to a fully explicit scheme when mass-lumping is applied, but cannot correctly represent corner singularities in general [8].

Discontinuous Galerkin (DG) FEMs offer an attractive alternative to edge elements for the numerical solution of Maxwell's equations, in particular for time-dependent problems. Not only do they accommodate elements of various types and shapes, irregular non-matching grids, and even locally varying polynomial order, and hence offer greater flexibility in the mesh design; they also lead to a block-diagonal mass matrix, with block size equal to the number of degrees of freedom per element. Thus when a spatial DG discretisation is combined with explicit time integration, the resulting time marching scheme will be truly explicit and inherently parallel.

☆ This work was supported by the Swiss National Science Foundation.
* Corresponding author.
E-mail addresses: Marcus.Grote@unibas.ch (M.J. Grote), Teodora.Mitkova@unibas.ch (T. Mitkova).

0377-0427/$ – see front matter © 2010 Elsevier B.V. All rights reserved.
doi:10.1016/j.cam.2010.04.028

For the time-dependent Maxwell equations in first-order hyperbolic form, various DG methods are available [10–13], which combine high order nodal elements with low-storage Runge–Kutta (RK) time integration. By using a strong-stability-preserving RK scheme instead, improved accuracy and a less stringent time-step restriction can be achieved [14]. For Maxwell's equations in second-order form, a symmetric interior penalty (IP) DG method was proposed in [15,16], which yields optimal a priori error estimates in the energy norm and in the L^2-norm. In a non-conducting source-free medium, it also conserves (a discrete version of) the energy.

In the presence of complex geometry, adaptivity and mesh refinement are certainly key for the efficient numerical solution of Maxwell's equations. However, locally refined meshes impose severe stability constraints on explicit time-stepping schemes, where the maximal time-step allowed by a CFL condition is dictated by the smallest elements in the mesh [17]. When mesh refinement is restricted to a small region, the use of implicit methods, or a very small time step in the entire computational domain, are very high a price to pay. To overcome this stability restriction, various local time-stepping schemes [18,19] were proposed, which use implicit time-stepping or explicit smaller time-steps only where the smallest elements in the mesh are located. However, straightforward interpolation or extrapolation from the coarse to the finer space–time grid, say, generally results in low accuracy and poor stability properties. By enforcing the conservation of energy, an important ingredient for stability, Collino and Joly proposed a second-order local time-stepping method for the wave equation [18] and for Maxwell's equations [20] in a non-conducting medium. Although their approach remains explicit inside the coarse and the fine mesh, it nevertheless requires at every time step the solution of a linear system at the interface between the two grids.

Since DG methods are inherently local, they are particularly well suited for the development of explicit local time-stepping schemes [21]. By combining the symplectic Störmer–Verlet method with a DG discretisation, Piperno derived a symplectic local time-stepping scheme for Maxwell's equations in a non-conducting medium [22], which is explicit and second-order accurate. In [23], Montseny et al. combined a similar recursive integrator with discontinuous hexahedral elements. Although hexahedral elements are very efficient, they can produce spurious modes [24] while automated grid generation only with such elements remains a non-trivial task. Starting from the standard leap-frog scheme, Diaz and Grote [25] devised an explicit energy conserving local time-stepping scheme of arbitrarily high accuracy for the homogeneous wave equation. Recently, Taube et al. [26] proposed an explicit local time-stepping method for Maxwell's equations by extending the so-called arbitrary high-order derivatives (ADER) DG approach to Maxwell's equations; there, the solution is expanded in Taylor series in time and then the Cauchy–Kovalevskaya procedure is used to replace the time derivatives in this series by space derivatives.

Here we derive explicit local time-stepping methods for Maxwell's equations in conducting or non-conducting media with source terms. The rest of the paper is organized as follows. In Section 2, we present the Maxwell equations in second-order form and briefly recall the symmetric IP–DG formulation from [15,16] Section 3. Starting from the well-known second-order leap-frog scheme, we then derive in Section 4 explicit second-order local time-stepping schemes both in a conducting and in a non-conducting medium. In a non-conducting medium, we show that (a discrete version of) the energy is conserved, which provides a rigorous criterion for numerical stability. By using the modified equation approach, we then derive in Section 5 explicit local time-stepping methods of arbitrarily high accuracy in a non-conducting medium. Finally in Section 6, we present several numerical experiments, which validate the theory and illustrate the usefulness of the proposed local time-stepping schemes.

2. The Maxwell equations

The evolution of a time-dependent electromagnetic field $\mathbf{E}(\mathbf{x}, t)$, $\mathbf{H}(\mathbf{x}, t)$ propagating through a linear isotropic medium is governed by Maxwell's equations:

$$\begin{aligned} \varepsilon \mathbf{E}_t &= \nabla \times \mathbf{H} - \sigma \mathbf{E} + \mathbf{j}, \\ \mu \mathbf{H}_t &= \nabla \times \mathbf{E}. \end{aligned}$$

Here, the coefficients μ, ε and σ denote the relative magnetic permeability, the relative electric permittivity and the conductivity of the medium, respectively. The source term $\mathbf{j}$ corresponds to the applied current density. By eliminating the magnetic field $\mathbf{H}$, Maxwell's equations reduce to a second-order vector wave equation for the electric field $\mathbf{E}$:

$$\varepsilon \mathbf{E}_{tt} + \sigma \mathbf{E}_t + \nabla \times (\mu^{-1} \nabla \times \mathbf{E}) = \mathbf{j}_t.$$

If the electric field is eliminated instead, one easily finds that the magnetic field $\mathbf{H}$ satisfies a similar vector wave equation. Thus, we consider the following model problem: find the (electric or magnetic) field $\mathbf{u}(\mathbf{x}, t)$ such that

$$\begin{aligned} &\varepsilon \mathbf{u}_{tt} + \sigma \mathbf{u}_t + \nabla \times (\mu^{-1} \nabla \times \mathbf{u}) = \mathbf{f} \quad \text{in } \Omega \times (0, T), \\ &\mathbf{n} \times \mathbf{u} = 0 \quad \text{on } \partial\Omega \times (0, T), \\ &\mathbf{u}(\cdot, 0) = \mathbf{u}_0 \quad \text{in } \Omega, \\ &\mathbf{u}_t(\cdot, 0) = \mathbf{v}_0 \quad \text{in } \Omega. \end{aligned} \tag{1}$$

Here, Ω is a bounded domain in $\mathbb{R}^d$, $d = 2, 3$, and $\mathbf{n}$ is the outward unit normal to the domain boundary $\partial\Omega$. The right-hand side $\mathbf{f}$ is a (known) source term in $L^2([0,T]; L^2(\Omega)^d)$. The functions $\mathbf{u}_0$ and $\mathbf{v}_0$ in (1) are prescribed initial data with $\mathbf{u}_0 \in H_0(\mathrm{curl};\Omega)$ and $\mathbf{v}_0 \in L^2(\Omega)^d$, where

$$H_0(\mathrm{curl};\Omega) = \{\mathbf{v} \in L^2(\Omega)^d : \nabla\times\mathbf{v} \in L^2(\Omega)^d, \mathbf{n}\times\mathbf{u} = 0 \text{ on } \partial\Omega\}.$$

We assume that the coefficients $\varepsilon = \varepsilon(\mathbf{x}) \geq \varepsilon_0$ and $\mu = \mu(\mathbf{x}) \geq \mu_0$ are strictly positive and uniformly bounded below, $\varepsilon_0, \mu_0 > 0$, and that $\sigma = \sigma(\mathbf{x})$ is non-negative, $\sigma \geq 0$. Then, the model problem (1) is well-posed and has a unique (weak) solution [27], $\mathbf{u} \in C^0(0,T; H_0(\mathrm{curl};\Omega)) \cap C^1(0,T; L^2(\Omega)^d)$.

3. Discontinuous Galerkin semi-discrete formulation

Here, we briefly recall the symmetric interior penalty (IP) DG formulation of (1) from [15,16]. We consider shape-regular meshes $\mathcal{T}_h$ that partition the domain Ω into disjoint triangles or tetrahedra K, such that $\overline{\Omega} = \cup_{K\in\mathcal{T}_h}\overline{K}$. For simplicity, we assume in this section that the elements are triangles in two space dimensions and tetrahedra in three space dimensions. Generally, we allow for irregular (k-irregular) meshes with hanging nodes [28]. The diameter of element K is denoted by h_K and the mesh size, h, is given by $h = \max_{K\in\mathcal{T}_h} h_K$. We denote by $\mathcal{E}_h^{\mathcal{I}}$ the set of all interior edges of $\mathcal{T}_h$, by $\mathcal{E}_h^{\mathcal{B}}$ the set of all boundary edges of $\mathcal{T}_h$, and set $\mathcal{E}_h = \mathcal{E}_h^{\mathcal{I}} \cup \mathcal{E}_h^{\mathcal{B}}$. Here, we generically refer to any element of $\mathcal{E}_h$ as an "edge", both in two and three space dimensions.

For a piecewise smooth vector-valued function $\mathbf{v}$, we introduce the following trace operators. Let $e \in \mathcal{E}_h^{\mathcal{I}}$ be an interior edge shared by two elements K^+ and K^- with unit outward normal vectors $\mathbf{n}^\pm$, respectively. Denoting by $\mathbf{v}^\pm$ the trace of $\mathbf{v}$ on $\partial K^\pm$ taken from within $K^\pm$, we define the jump and the average on e by

$$[\![\mathbf{v}]\!] := \mathbf{n}^+\times\mathbf{v}^+ + \mathbf{n}^-\times\mathbf{v}^-, \qquad \{\!\{\mathbf{v}\}\!\} := (\mathbf{v}^+ + \mathbf{v}^-)/2.$$

On every boundary edge $e \in \mathcal{E}_h^{\mathcal{B}}$, we set

$$[\![\mathbf{v}]\!] := \mathbf{n}\times\mathbf{v} \quad \text{and} \quad \{\!\{\mathbf{v}\}\!\} := \mathbf{v}.$$

For a given partition $\mathcal{T}_h$ of Ω and an approximation order $\ell \geq 1$, we shall approximate the solution $\mathbf{u}(\cdot,t)$ of (1) in the finite element space

$$\mathbf{V}^h = \left\{\mathbf{v} \in L^2(\Omega)^d : \mathbf{v}|_K \in \mathcal{P}^\ell(K)^d, \ \forall K \in \mathcal{T}_h\right\},$$

where $\mathcal{P}^\ell(K)$ denotes the space of polynomials of total degree at most ℓ on K. Thus, we consider the following (semi-discrete) discontinuous Galerkin finite element formulation [15,16]: find $\mathbf{u}^h : [0,T] \to \mathbf{V}^h$ such that

$$\begin{aligned} &(\varepsilon\mathbf{u}_{tt}^h, \mathbf{v}) + (\sigma\mathbf{u}_t^h, \mathbf{v}) + a_h(\mathbf{u}^h, \mathbf{v}) = (\mathbf{f}, \mathbf{v}), \quad \forall\mathbf{v} \in \mathbf{V}^h, \ t \in (0,T),\\ &\mathbf{u}^h(\cdot,0) = \boldsymbol{\Pi}_h\mathbf{u}_0,\\ &\mathbf{u}_t^h(\cdot,0) = \boldsymbol{\Pi}_h\mathbf{v}_0. \end{aligned} \tag{2}$$

Here $\boldsymbol{\Pi}_h$ is the L^2-projection onto $\mathbf{V}^h$. The discrete bilinear form $a_h(\cdot,\cdot)$, defined on $\mathbf{V}^h \times \mathbf{V}^h$, is given by

$$\begin{aligned} a_h(\mathbf{u},\mathbf{v}) = &\sum_{K\in\mathcal{T}_h}\int_K \mu^{-1}(\nabla\times\mathbf{u})\cdot(\nabla\times\mathbf{v})\,\mathrm{d}\mathbf{x} - \sum_{e\in\mathcal{E}_h}\int_e [\![\mathbf{v}]\!]\cdot\{\!\{\mu^{-1}\nabla\times\mathbf{u}\}\!\}\,\mathrm{d}A\\ &- \sum_{e\in\mathcal{E}_h}\int_e [\![\mathbf{u}]\!]\{\!\{\mu^{-1}\nabla\times\mathbf{v}\}\!\}\,\mathrm{d}A + \sum_{e\in\mathcal{E}_h}\int_e \mathtt{a}[\![\mathbf{u}]\!]\cdot[\![\mathbf{v}]\!]\,\mathrm{d}A. \end{aligned}$$

The function $\mathtt{a}$ penalizes the jumps of $\mathbf{u}$ and $\mathbf{v}$ over the edges of $\mathcal{T}_h$. To define it, we first introduce the functions $\mathtt{h}$ and $\mathtt{m}$ by

$$\mathtt{h}|_e = \begin{cases} \min\{h_{K^+}, h_{K^-}\}, & e \in \mathcal{E}_h^{\mathcal{I}},\\ h_K, & e \in \mathcal{E}_h^{\mathcal{B}}, \end{cases} \qquad \mathtt{m}|_e = \begin{cases} \min\{\mu_{K^+}, \mu_{K^-}\}, & e \in \mathcal{E}_h^{\mathcal{I}},\\ \mu_K, & e \in \mathcal{E}_h^{\mathcal{B}}. \end{cases}$$

Then, on each $e \in \mathcal{E}_h$, we set

$$\mathtt{a}|_e := \alpha\mathtt{m}^{-1}\mathtt{h}^{-1}, \tag{3}$$

where α is a positive parameter independent of the local mesh sizes. There exists a threshold value $\alpha_{\min} > 0$, independent of the local mesh size, such that for $\alpha \geq \alpha_{\min}$ the discontinuous Galerkin bilinear form $a_h(\cdot,\cdot)$ is coercive [29,30]. Hence, the semi-discrete problem (2) is well-posed and uniquely solvable provided that $\alpha \geq \alpha_{\min}$. This completes the semi-discrete formulation of the IP–DG method for (1).

In [15,16], a detailed convergence analysis and numerical study of the semi-discrete problem (2) was presented. In particular, optimal a priori estimates in a DG-energy norm were derived, either for smooth solutions on arbitrary meshes or

for low regularity (singular) solutions on conforming meshes [15]. For sufficiently smooth solutions on regular tetrahedral meshes, the above IP–DG method (2) also yields the optimal L^2-error estimate [16]

$$\|\mathbf{u} - \mathbf{u}^h\|_{L^\infty(0,T;L^2(\Omega)^d)} \leq Ch^{\ell+1},$$

where the constant $C = C(\Omega, \mathbf{u}, T) > 0$ is independent of the mesh size.

The semi-discrete IP–DG formulation (2) is equivalent to the second-order system of ordinary differential equations

$$\mathbf{M}_\varepsilon \frac{\mathrm{d}^2\mathbf{U}}{\mathrm{d}t^2}(t) + \mathbf{M}_\sigma \frac{\mathrm{d}\mathbf{U}}{\mathrm{d}t}(t) + \mathbf{K}\mathbf{U}(t) = \mathbf{F}(t), \quad t \in (0,T),$$

with initial conditions

$$\mathbf{M}\mathbf{U}(0) = \mathbf{u}_0^h, \qquad \mathbf{M}\frac{\mathrm{d}\mathbf{U}}{\mathrm{d}t}(0) = \mathbf{v}_0^h.$$

Here $\mathbf{U}$ denotes the vector whose components are the coefficients of $\mathbf{u}^h$ with respect to the finite element basis of $\mathbf{V}_h$, $\mathbf{M}$ the mass matrix, $\mathbf{K}$ the DG stiffness matrix, and $\mathbf{M}_\varepsilon$, $\mathbf{M}_\sigma$ denote the mass matrices with weights ε, σ, respectively. Because individual elements decouple, the mass matrices are sparse, symmetric, positive definite, and block-diagonal with block size equal to the number of degrees of freedom per element. Thus, they can be inverted at very low computational cost. In fact, for a judicious choice of (locally orthogonal) shape functions, the mass matrices are truly diagonal. The stiffness matrix $\mathbf{K}$ is sparse, symmetric and, in general, positive semi-definite.

4. Second-order explicit local time-stepping

We consider the semi-discrete model equation

$$\mathbf{M}_\varepsilon \frac{\mathrm{d}^2\mathbf{U}}{\mathrm{d}t^2} + \mathbf{M}_\sigma \frac{\mathrm{d}\mathbf{U}}{\mathrm{d}t} + \mathbf{K}\mathbf{U} = \mathbf{F}, \tag{4}$$

where $\mathbf{M}_\varepsilon$ and $\mathbf{M}_\sigma$ are symmetric positive definite matrices and $\mathbf{K}$ is a symmetric positive semi-definite matrix; moreover, we assume that the mass matrix $\mathbf{M}_\varepsilon$ is (block-)diagonal, as in the IP–DG formulation (2). We remark, however, that the time integration techniques presented below are also applicable to other spatial discretisations of Maxwell's equations that lead to the same semi-discrete form (4).

Because $\mathbf{M}_\varepsilon$ is assumed block-diagonal, $\mathbf{M}_\varepsilon^{\frac{1}{2}}$ can be explicitly computed and inverted at low cost. Thus, we multiply (4) by $\mathbf{M}_\varepsilon^{-\frac{1}{2}}$ to obtain

$$\frac{\mathrm{d}^2\mathbf{z}}{\mathrm{d}t^2} + \mathbf{D}\frac{\mathrm{d}\mathbf{z}}{\mathrm{d}t} + \mathbf{A}\mathbf{z} = \mathbf{R}, \tag{5}$$

with $\mathbf{z} = \mathbf{M}_\varepsilon^{\frac{1}{2}}\mathbf{U}$, $\mathbf{D} = \mathbf{M}_\varepsilon^{-\frac{1}{2}}\mathbf{M}_\sigma\mathbf{M}_\varepsilon^{-\frac{1}{2}}$, $\mathbf{A} = \mathbf{M}_\varepsilon^{-\frac{1}{2}}\mathbf{K}\mathbf{M}_\varepsilon^{-\frac{1}{2}}$ and $\mathbf{R} = \mathbf{M}_\varepsilon^{-\frac{1}{2}}\mathbf{F}$. Note that $\mathbf{A}$ is also sparse and symmetric positive semidefinite. In a non-conducting medium, $\mathbf{D}$ vanishes and hence energy is conserved, whereas in a conducting medium $\mathbf{D}$ is nonzero and energy is dissipated. We shall distinguish these two situations in the derivation of local time-stepping schemes below.

4.1. Local time-stepping method in a non-conducting medium

In a non-conducting medium, (5) reduces to

$$\frac{\mathrm{d}^2\mathbf{z}}{\mathrm{d}t^2} + \mathbf{A}\mathbf{z} = \mathbf{R}. \tag{6}$$

Since for any $f \in \mathcal{C}^2$, we have

$$f(t+\Delta t) - 2f(t) + f(t-\Delta t) = \Delta t^2 \int_{-1}^{1} (1-|\theta|) f''(t+\theta\Delta t)\,\mathrm{d}\theta, \tag{7}$$

the exact solution $\mathbf{z}(t)$ of (6) satisfies

$$\mathbf{z}(t+\Delta t) - 2\mathbf{z}(t) + \mathbf{z}(t-\Delta t) = \Delta t^2 \int_{-1}^{1} (1-|\theta|)\,(\mathbf{R}(t+\theta\Delta t) - \mathbf{A}\mathbf{z}(t+\theta\Delta t))\,\mathrm{d}\theta. \tag{8}$$

The integral on the right side of (8) represents a weighted average of $\mathbf{R}(s) - \mathbf{A}\mathbf{z}(s)$ over the interval $[t-\Delta t, t+\Delta t]$, which needs to be approximated in any numerical algorithm. If we approximate in (8) $\mathbf{A}\mathbf{z}(t+\theta\Delta t)$ and $\mathbf{R}(t+\theta\Delta t)$ by $\mathbf{A}\mathbf{z}(t)$

and $\mathbf{R}(t)$, respectively, and evaluate the remaining θ-dependent integral, we obtain the well-known second-order leap-frog scheme with time-step Δt,

$$\mathbf{z}_{n+1} - 2\mathbf{z}_n + \mathbf{z}_{n-1} = \Delta t^2 \left(\mathbf{R}_n - \mathbf{A}\mathbf{z}_n\right), \quad \mathbf{R}_n \simeq \mathbf{R}(t_n),\ \mathbf{z}_n \simeq \mathbf{z}(t_n), \tag{9}$$

which, however, would require Δt to be comparable in size to the smallest elements in the mesh for numerical stability.

Following [25,31], we instead split the vectors $\mathbf{z}(t)$ and $\mathbf{R}(t)$ as

$$\begin{aligned} \mathbf{z}(t) &= (\mathbf{I}-\mathbf{P})\mathbf{z}(t) + \mathbf{P}\mathbf{z}(t) = \mathbf{z}^{[\text{coarse}]}(t) + \mathbf{z}^{[\text{fine}]}(t), \\ \mathbf{R}(t) &= (\mathbf{I}-\mathbf{P})\mathbf{R}(t) + \mathbf{P}\mathbf{R}(t) = \mathbf{R}^{[\text{coarse}]}(t) + \mathbf{R}^{[\text{fine}]}(t), \end{aligned} \tag{10}$$

where the projection matrix $\mathbf{P}$ is diagonal. Its diagonal entries, equal to zero or one, identify the unknowns associated with the locally refined region, where smaller time-steps are needed. To circumvent the severe CFL restriction on Δt in the leap-frog scheme, we need to treat $\mathbf{z}^{[\text{fine}]}(t)$ and $\mathbf{R}^{[\text{fine}]}(t)$ differently from $\mathbf{z}^{[\text{coarse}]}(t)$ and $\mathbf{R}^{[\text{coarse}]}(t)$ in

$$\begin{aligned} \mathbf{z}(t+\Delta t) - 2\mathbf{z}(t) + \mathbf{z}(t-\Delta t) = \Delta t^2 \int_{-1}^{1} (1-|\theta|) \big\{ &\mathbf{R}^{[\text{coarse}]}(t+\theta\Delta t) + \mathbf{R}^{[\text{fine}]}(t+\theta\Delta t) \\ &- \mathbf{A}\left(\mathbf{z}^{[\text{coarse}]}(t+\theta\Delta t) + \mathbf{z}^{[\text{fine}]}(t+\theta\Delta t)\right)\big\}\, \mathrm{d}\theta. \end{aligned} \tag{11}$$

Since we wish to use the standard leap-frog scheme in the coarse part of the mesh, we approximate the terms in (11) that involve $\mathbf{z}^{[\text{coarse}]}(t+\theta\Delta t)$ and $\mathbf{R}^{[\text{coarse}]}(t+\theta\Delta t)$ by their values at t, which yields

$$\begin{aligned} \mathbf{z}(t+\Delta t) - 2\mathbf{z}(t) + \mathbf{z}(t-\Delta t) \simeq\ & \Delta t^2 \left\{(\mathbf{I}-\mathbf{P})\mathbf{R}(t) - \mathbf{A}(\mathbf{I}-\mathbf{P})\mathbf{z}(t)\right\} \\ &+ \Delta t^2 \int_{-1}^{1} (1-|\theta|) \left\{\mathbf{P}\mathbf{R}(t+\theta\Delta t) - \mathbf{A}\mathbf{P}\mathbf{z}(t+\theta\Delta t)\right\} \mathrm{d}\theta. \end{aligned} \tag{12}$$

Note that $\mathbf{A}$ and $\mathbf{P}$ do not commute.

Next for fixed t, let $\widetilde{\mathbf{z}}(\tau)$ solve the differential equation

$$\begin{aligned} &\frac{\mathrm{d}^2\widetilde{\mathbf{z}}}{\mathrm{d}\tau^2}(\tau) = (\mathbf{I}-\mathbf{P})\mathbf{R}(t) - \mathbf{A}(\mathbf{I}-\mathbf{P})\mathbf{z}(t) + \mathbf{P}\mathbf{R}(t+\tau) - \mathbf{A}\mathbf{P}\widetilde{\mathbf{z}}(\tau), \\ &\widetilde{\mathbf{z}}(0) = \mathbf{z}(t), \\ &\widetilde{\mathbf{z}}'(0) = \nu, \end{aligned} \tag{13}$$

where ν will be specified below. Again from (7), we deduce that

$$\begin{aligned} \widetilde{\mathbf{z}}(\Delta t) - 2\widetilde{\mathbf{z}}(0) + \widetilde{\mathbf{z}}(-\Delta t) =\ & \Delta t^2 \left\{(\mathbf{I}-\mathbf{P})\mathbf{R}(t) - \mathbf{A}(\mathbf{I}-\mathbf{P})\mathbf{z}(t)\right\} \\ &+ \Delta t^2 \int_{-1}^{1} (1-|\theta|) \left\{\mathbf{P}\mathbf{R}(t+\theta\Delta t) - \mathbf{A}\mathbf{P}\widetilde{\mathbf{z}}(\theta\Delta t)\right\} \mathrm{d}\theta. \end{aligned} \tag{14}$$

From the comparison of (12) with (14), we infer that

$$\mathbf{z}(t+\Delta t) - 2\mathbf{z}(t) + \mathbf{z}(t-\Delta t) \simeq \widetilde{\mathbf{z}}(\Delta t) - 2\widetilde{\mathbf{z}}(0) + \widetilde{\mathbf{z}}(-\Delta t),$$

or equivalently

$$\mathbf{z}(t+\Delta t) + \mathbf{z}(t-\Delta t) \simeq \widetilde{\mathbf{z}}(\Delta t) + \widetilde{\mathbf{z}}(-\Delta t). \tag{15}$$

In fact from Taylor expansion and (6), we obtain

$$\begin{aligned} \widetilde{\mathbf{z}}(\Delta t) + \widetilde{\mathbf{z}}(-\Delta t) &= 2\widetilde{\mathbf{z}}(0) + \widetilde{\mathbf{z}}''(0)\Delta t^2 + \mathcal{O}(\Delta t^4) = 2\mathbf{z}(t) + (\mathbf{R}(t) - \mathbf{A}\mathbf{z}(t))\Delta t^2 + \mathcal{O}(\Delta t^4) \\ &= \mathbf{z}(t+\Delta t) + \mathbf{z}(t-\Delta t) + \mathcal{O}(\Delta t^4). \end{aligned}$$

Thus to advance $\mathbf{z}(t)$ from t to $t+\Delta t$, we shall evaluate $\widetilde{\mathbf{z}}(\Delta t) + \widetilde{\mathbf{z}}(-\Delta t)$ by solving (13) numerically.

To take advantage of the inherent symmetry in time and thereby reduce the computational effort even further, we now let

$$\mathbf{q}(\tau) = \widetilde{\mathbf{z}}(\tau) + \widetilde{\mathbf{z}}(-\tau).$$

Then, $q(\tau)$ solves the differential equation

$$\begin{aligned} &\frac{\mathrm{d}^2\mathbf{q}}{\mathrm{d}\tau^2}(\tau) = 2\left\{(\mathbf{I}-\mathbf{P})\mathbf{R}(t) - \mathbf{A}(\mathbf{I}-\mathbf{P})\mathbf{z}(t)\right\} + \mathbf{P}\left\{\mathbf{R}(t+\tau) + \mathbf{R}(t-\tau)\right\} - \mathbf{A}\mathbf{P}\mathbf{q}(\tau), \\ &\mathbf{q}(0) = 2\mathbf{z}(t), \\ &\mathbf{q}'(0) = 0, \end{aligned} \tag{16}$$

with

$$\mathbf{z}(t+\Delta t)+\mathbf{z}(t-\Delta t)=\mathbf{q}(\Delta t)+\mathcal{O}(\Delta t^4). \tag{17}$$

Note that $\mathbf{q}(\Delta t)$ does not depend on the value of ν. Now, we shall approximate the right side of (8) by solving (16) on $[0,\ \Delta t]$, and then use (17) to compute $\mathbf{z}(t+\Delta t)$. Thus, we need the numerical value of $\mathbf{q}(\tau)$ only at Δt. Clearly, in doing so we must also ensure that the overall numerical scheme remains second-order accurate in time, as we shall show below.

In summary, the local time-stepping algorithm for the solution of (6) computes $\mathbf{z}_{n+1}\simeq\mathbf{z}(t+\Delta t)$, given $\mathbf{z}_n$ and $\mathbf{z}_{n-1}$, as follows:

Algorithm 1. 1. Set $\mathbf{w}:=(\mathbf{I}-\mathbf{P})\mathbf{R}_n-\mathbf{A}(\mathbf{I}-\mathbf{P})\mathbf{z}_n$ and $\mathbf{q}_0:=2\mathbf{z}_n$.

2. Compute $\mathbf{q}_{1/p}:=\mathbf{q}_0+\frac{1}{2}\left(\frac{\Delta t}{p}\right)^2\left(2\mathbf{w}+2\mathbf{P}\mathbf{R}_{n,0}-\mathbf{A}\mathbf{P}\mathbf{q}_0\right)$.

3. For $m=1,\ldots,p-1$, compute

$$\mathbf{q}_{(m+1)/p}:=2\mathbf{q}_{m/p}-\mathbf{q}_{(m-1)/p}+\left(\frac{\Delta t}{p}\right)^2\left(2\mathbf{w}+\mathbf{P}(\mathbf{R}_{n,m}+\mathbf{R}_{n,-m})-\mathbf{A}\mathbf{P}\mathbf{q}_{m/p}\right). \tag{18}$$

4. Compute $\mathbf{z}_{n+1}:=-\mathbf{z}_{n-1}+\mathbf{q}_1$.

Here, we have used the notations $\mathbf{R}_{n,m}\simeq\mathbf{R}(t_n+\tau_m)$ and $\mathbf{R}_{n,-m}\simeq\mathbf{R}(t_n-\tau_m)$, where $t_n=n\Delta t$ and $\tau_m=m\Delta\tau$; note that $\mathbf{R}_{n,0}\simeq\mathbf{R}(t_n+\tau_0)=\mathbf{R}(t_n)\simeq\mathbf{R}_n$. Steps 1–3 correspond to the numerical solution of (16) until $\tau=\Delta t$ with the leap-frog scheme, using the local time-step $\Delta\tau=\Delta t/p$. For $\mathbf{P}=\mathbf{0}$, that is without any local time-stepping, we recover the standard leap-frog scheme. If the fraction of nonzero entries in $\mathbf{P}$ is small, the overall cost is dominated by the computation of $\mathbf{w}$, which requires one multiplication by $\mathbf{A}(\mathbf{I}-\mathbf{P})$ per time-step Δt. All further matrix–vector multiplications by $\mathbf{AP}$ only affect those unknowns that lie inside the refined region, or immediately next to it.

We are now ready to establish the accuracy of the above local time-stepping scheme. We begin by proving the following two technical results.

Lemma 1. *For $m\geq 2$, $\mathbf{q}_{m/p}$ defined by Algorithm 1 satisfies*

$$\mathbf{q}_{m/p}=2\mathbf{z}_n+\left(\frac{\Delta t}{p}\right)^2\left(m^2(\mathbf{R}_{n,0}-\mathbf{A}\mathbf{z}_n)+\mathbf{P}\mathcal{R}_m\right)+\mathcal{O}\left(\Delta t^4\right), \tag{19}$$

where the terms $\mathcal{R}_m$ are given by

$$\begin{aligned}
&\mathcal{R}_2=\mathbf{R}_{n,1}+\mathbf{R}_{n,-1}-2\mathbf{R}_{n,0},\\
&\mathcal{R}_3=2\mathcal{R}_2+\mathbf{R}_{n,2}+\mathbf{R}_{n,-2}-2\mathbf{R}_{n,0},\\
&\mathcal{R}_m=2\mathcal{R}_{m-1}-\mathcal{R}_{m-2}+\mathbf{R}_{n,m-1}+\mathbf{R}_{n,-(m-1)}-2\mathbf{R}_{n,0}\quad\forall m\geq 4.
\end{aligned} \tag{20}$$

Proof. The proof is by induction on m. We first show that (19) holds for $m=2,3$. Since

$$\mathbf{q}_{1/p}=\mathbf{q}_0+\frac{1}{2}\left(\frac{\Delta t}{p}\right)^2\left(2\mathbf{w}+2\mathbf{P}\mathbf{R}_{n,0}-\mathbf{A}\mathbf{P}\mathbf{q}_0\right)=2\mathbf{z}_n+\left(\frac{\Delta t}{p}\right)^2\left(\mathbf{R}_{n,0}-\mathbf{A}\mathbf{z}_n\right),$$

we find from (18) with $m=1$ that

$$\mathbf{q}_{2/p}=2\mathbf{z}_n+\left(\frac{\Delta t}{p}\right)^2\left(4\mathbf{R}_{n,0}-4\mathbf{A}\mathbf{z}_n+\mathbf{P}(\mathbf{R}_{n,1}+\mathbf{R}_{n,-1}-2\mathbf{R}_{n,0})\right)-\left(\frac{\Delta t}{p}\right)^4\left(\mathbf{A}\mathbf{P}\mathbf{R}_{n,0}-\mathbf{A}\mathbf{P}\mathbf{A}\mathbf{z}_n\right),$$

which yields (19) with $\mathcal{R}_2$ as in (20). The case $m=3$ follows by a similar argument.

Next, let (19) hold for $m\geq 3$. From (18) we then have

$$\begin{aligned}
\mathbf{q}_{(m+1)/p}=\ &2\left(2\mathbf{z}_n+\left(\frac{\Delta t}{p}\right)^2\left(m^2\left(\mathbf{R}_{n,0}-\mathbf{A}\mathbf{z}_n\right)+\mathbf{P}\mathcal{R}_m\right)\right)-2\mathbf{z}_n-\left(\frac{\Delta t}{p}\right)^2\left((m-1)^2\left(\mathbf{R}_{n,0}-\mathbf{A}\mathbf{z}_n\right)+\mathbf{P}\mathcal{R}_{m-1}\right)\\
&+\left(\frac{\Delta t}{p}\right)^2\left\{2(\mathbf{I}-\mathbf{P})\mathbf{R}_{n,0}-2\mathbf{A}(\mathbf{I}-\mathbf{P})\mathbf{z}_n+\mathbf{P}(\mathbf{R}_{n,m}+\mathbf{R}_{n,-m})-2\mathbf{A}\mathbf{P}\mathbf{z}_n\right\}+\mathcal{O}\left(\Delta t^4\right).
\end{aligned}$$

After simplification, we find

$$\mathbf{q}_{(m+1)/p}=2\mathbf{z}_n+\left(\frac{\Delta t}{p}\right)^2\left\{(m+1)^2\left(\mathbf{R}_{n,0}-\mathbf{A}\mathbf{z}_n\right)+\mathbf{P}\left(2\mathcal{R}_m-\mathcal{R}_{m-1}+\mathbf{R}_{n,m}+\mathbf{R}_{n,-m}-2\mathbf{R}_{n,0}\right)\right\}+\mathcal{O}\left(\Delta t^4\right),$$

which corresponds to (19) and (20) with m replaced by $m+1$, and thus concludes the proof. □

Lemma 2. *For $m \geq 2$, we have*

$$\mathcal{R}_m = \sum_{k=1}^{m-1} k\mathbf{R}_{n,-(m-k)} - m(m-1)\mathbf{R}_{n,0} + \sum_{k=1}^{m-1} k\mathbf{R}_{n,m-k}, \tag{21}$$

with $\mathcal{R}_m$ defined by (20). Moreover, if $\mathbf{R}(t) \in C^2([0,T])$, we have

$$\mathcal{R}_m = \mathcal{O}\left(\Delta t^2\right), \quad \Delta t \to 0. \tag{22}$$

Proof. The proof of (21) is by induction on m. For $m = 2$ the statement clearly holds because of (20). For $m = 3$, we immediately find from (20) that

$$\mathcal{R}_3 = \mathbf{R}_{n,-2} + 2\mathbf{R}_{n,-1} - 6\mathbf{R}_{n,0} + 2\mathbf{R}_{n,1} + \mathbf{R}_{n,2}.$$

Now, let (21) holds for $m-1$ and m. Then,

$$\begin{aligned}\mathcal{R}_{m+1} = &\sum_{k=1}^{m-1} 2k\mathbf{R}_{n,-(m-k)} - 2m(m-1)\mathbf{R}_{n,0} + \sum_{k=1}^{m-1} 2k\mathbf{R}_{n,m-k} - \sum_{k=1}^{m-2} k\mathbf{R}_{n,-(m-1-k)}\\ &+ (m-1)(m-2)\mathbf{R}_{n,0} - \sum_{k=1}^{m-2} k\mathbf{R}_{n,m-1-k} + \mathbf{R}_{n,m} + \mathbf{R}_{n,-m} - 2\mathbf{R}_{n,0}.\end{aligned}$$

Rearranging terms we find

$$\begin{aligned}\mathcal{R}_{m+1} &= \sum_{\ell=2}^{m} 2(\ell-1)\mathbf{R}_{n,-(m+1-\ell)} + \sum_{\ell=2}^{m} 2(\ell-1)\mathbf{R}_{n,m+1-\ell} - \sum_{\ell=3}^{m}(\ell-2)\mathbf{R}_{n,-(m+1-\ell)}\\ &\quad - \sum_{\ell=3}^{m}(\ell-2)\mathbf{R}_{n,m+1-\ell} + \mathbf{R}_{n,m} + \mathbf{R}_{n,-m} - (2m(m-1) - (m-1)(m-2) + 2)\mathbf{R}_{n,0}\\ &= \sum_{\ell=1}^{m} \ell\mathbf{R}_{n,-(m+1-\ell)} - (m+1)m\mathbf{R}_{n,0} + \sum_{\ell=1}^{m} \ell\mathbf{R}_{n,m+1-\ell},\end{aligned}$$

which yields (21) after further simplifications.

To prove (22), we first show that

$$\mathcal{R}_m = \frac{m(m-1)}{2}\left(\mathbf{R}_{n,-1} - 2\mathbf{R}_{n,0} + \mathbf{R}_{n,1}\right) + \mathcal{O}\left(\Delta\tau^2\right), \tag{23}$$

with $m \geq 2$ and $\Delta\tau = \Delta t/p$. Replacing $\mathbf{R}_{n,-(m-k)}$ and $\mathbf{R}_{n,m-k}$ in (21) by their Taylor expansion

$$\begin{aligned}\mathbf{R}_{n,-(m-k)} &= \mathbf{R}_{n,-1} - (m-k-1)\Delta\tau\frac{\mathrm{d}\mathbf{R}}{\mathrm{d}t}(t_n - \Delta\tau) + \mathcal{O}\left(\Delta\tau^2\right),\\ \mathbf{R}_{n,m-k} &= \mathbf{R}_{n,1} + (m-k-1)\Delta\tau\frac{\mathrm{d}\mathbf{R}}{\mathrm{d}t}(t_n + \Delta\tau) + \mathcal{O}\left(\Delta\tau^2\right),\end{aligned}$$

we find that

$$\begin{aligned}\mathcal{R}_m = &\frac{m(m-1)}{2}\mathbf{R}_{n,-1} - m(m-1)\mathbf{R}_{n,0} + \frac{m(m-1)}{2}\mathbf{R}_{n,1}\\ &+ \sum_{k=1}^{m-1} k(m-k-1)\Delta\tau\left(\frac{\mathrm{d}\mathbf{R}}{\mathrm{d}t}(t_n + \Delta\tau) - \frac{\mathrm{d}\mathbf{R}}{\mathrm{d}t}(t_n - \Delta\tau)\right) + \mathcal{O}\left(\Delta\tau^2\right).\end{aligned}$$

Since

$$\frac{\mathrm{d}\mathbf{R}}{\mathrm{d}t}(t_n + \Delta\tau) - \frac{\mathrm{d}\mathbf{R}}{\mathrm{d}t}(t_n - \Delta\tau) = \mathcal{O}\left(\Delta\tau\right), \quad \Delta\tau \to 0,$$

(23) follows. Finally, since the first term on the right of (23) corresponds to the second-order central finite difference approximation for $\mathbf{R}''(t_n)$, we immediately obtain (22). □

We are now ready to establish the accuracy of the above local time-stepping scheme.

Proposition 1. *For $\mathbf{R}(t) \in C^2([0,T])$, the local time-stepping method (Algorithm 1) is second-order accurate.*

Proof. Recall that $\mathbf{z}_{n+1} = -\mathbf{z}_{n-1} + \mathbf{q}_1$. We now use (19) in Lemma 1 with $m = p$ to replace $\mathbf{q}_1$. This yields

$$\mathbf{z}_{n+1} = -\mathbf{z}_{n-1} + 2\mathbf{z}_n + \Delta t^2 \left(\mathbf{R}_{n,0} - \mathbf{A}\mathbf{z}_n\right) + \left(\frac{\Delta t}{p}\right)^2 \mathbf{P}\mathcal{R}_p + \mathcal{O}\left(\Delta t^4\right),$$

which is equivalent to

$$\frac{\mathbf{z}_{n+1} - 2\mathbf{z}_n + \mathbf{z}_{n-1}}{\Delta t^2} + \mathbf{A}\mathbf{z}_n = \mathbf{R}_{n,0} + \frac{1}{p^2}\mathbf{P}\mathcal{R}_p + \mathcal{O}\left(\Delta t^2\right).$$

From (22) in Lemma 2 with $m = p$ and the comparison with (6), we conclude that the local time-stepping scheme is second-order accurate. □

To establish the stability of the above local time-stepping scheme we consider the homogeneous case, $\mathbf{R} = \mathbf{0}$. Then, the standard leap-frog scheme (9) conserves the discrete energy

$$E^{n+\frac{1}{2}} = \frac{1}{2}\left[\left\langle\left(\mathbf{I} - \frac{\Delta t^2}{4}\mathbf{A}\right)\frac{\mathbf{z}_{n+1} - \mathbf{z}_n}{\Delta t}, \frac{\mathbf{z}_{n+1} - \mathbf{z}_n}{\Delta t}\right\rangle + \left\langle\mathbf{A}\frac{\mathbf{z}_{n+1} + \mathbf{z}_n}{2}, \frac{\mathbf{z}_{n+1} + \mathbf{z}_n}{2}\right\rangle\right]. \tag{24}$$

Here $E^{n+\frac{1}{2}} \simeq E(t_{n+\frac{1}{2}})$ and the angular brackets denote the standard Euclidean inner product. Since $\mathbf{A}$ is symmetric, the quadratic form in (24) is also symmetric. For sufficiently small Δt it is also positive semidefinite and hence yields a true energy.

To derive a necessary and sufficient condition for the numerical stability of the local time-stepping scheme, we shall also exhibit a conserved discrete energy for Algorithm 1 with $\mathbf{R}_n = \mathbf{0}$. Following [25], we first show how to rewrite the local time-stepping Algorithm 1 in "leap-frog manner". To do so, we need the following technical result.

Lemma 3. *For $m \geq 2$, $\mathbf{q}_{m/p}$ defined in (18) with $\mathbf{R}_{n,m} = \mathbf{0}$ satisfies*

$$\mathbf{q}_{m/p} = 2\mathbf{z}_n - m^2\left(\frac{\Delta t}{p}\right)^2 \mathbf{A}\mathbf{z}_n + \sum_{j=1}^{m-1}\left(\frac{\Delta t}{p}\right)^{2(j+1)} \alpha_j^m (\mathbf{A}\mathbf{P})^j \mathbf{A}\mathbf{z}_n, \tag{25}$$

where the constants α_j^m are given by

$$\begin{aligned}
&\alpha_1^2 = 1, \qquad \alpha_1^3 = 6, \qquad \alpha_2^3 = -1,\\
&\alpha_1^{m+1} = m^2 + 2\alpha_1^m - \alpha_1^{m-1},\\
&\alpha_j^{m+1} = 2\alpha_j^m - \alpha_j^{m-1} - \alpha_{j-1}^m, \quad j = 2, \ldots, m-2,\\
&\alpha_{m-1}^{m+1} = 2\alpha_{m-1}^m - \alpha_{m-2}^m,\\
&\alpha_m^{m+1} = -\alpha_{m-1}^m.
\end{aligned} \tag{26}$$

Proof. The proof is by induction on m. As it is similar to the proof of Lemma 3.2 in [25], we refrain from repeating it here; however, we note that the constants α_j^p in (26) are not identical to those in [25]. □

As a consequence, we can rewrite the local time-stepping algorithm in "leap-frog manner".

Proposition 2. *The local time-stepping scheme (Algorithm 1) with $\mathbf{R}_{n,m} = \mathbf{0}$ is equivalent to*

$$\mathbf{z}_{n+1} = 2\mathbf{z}_n - \mathbf{z}_{n-1} - \Delta t^2 \mathbf{A}_p \mathbf{z}_n,$$

where $\mathbf{A}_p$ is defined by

$$\mathbf{A}_p = \mathbf{A} - \frac{2}{p^2}\sum_{j=1}^{p-1}\left(\frac{\Delta t}{p}\right)^{2j} \alpha_j^p (\mathbf{A}\mathbf{P})^j \mathbf{A} \tag{27}$$

and the constants α_j^p are given by (26). Furthermore, the matrix $\mathbf{A}_p$ is symmetric.

Proof. Starting from the definition of $\mathbf{q}_1 = \mathbf{q}_{p/p}$ in (18), the result immediately follows from (27) and Lemma 3 with $m = p$. The symmetry of $\mathbf{A}_p$ follows from the symmetry of $\mathbf{A}$ and $\mathbf{P}$. □

Remark 1. Proposition 2 is required for the stability analysis. However, the actual implementation of the local time-stepping scheme follows Algorithm 1. In particular, neither $\mathbf{A}_p$ nor the constants α_j^p are ever used in practice.

Proposition 3. *The local time-stepping scheme (Algorithm 1) with* $\mathbf{R}_n = \mathbf{0}$ *conserves the energy*

$$E^{n+\frac{1}{2}} = \frac{1}{2}\left[\left\langle\left(\mathbf{I} - \frac{\Delta t^2}{4}\mathbf{A}_p\right)\frac{\mathbf{z}_{n+1}-\mathbf{z}_n}{\Delta t}, \frac{\mathbf{z}_{n+1}-\mathbf{z}_n}{\Delta t}\right\rangle + \left\langle \mathbf{A}_p \frac{\mathbf{z}_{n+1}+\mathbf{z}_n}{2}, \frac{\mathbf{z}_{n+1}+\mathbf{z}_n}{2}\right\rangle\right]. \tag{28}$$

Proof. By symmetry of $\mathbf{A}_p$, this classical proof is similar to that of (24); see also [25] for details. □

The above local time-stepping scheme (Algorithm 1) with $\mathbf{R}_n = \mathbf{0}$ conserves the energy $E^{n+\frac{1}{2}}$ in (28), which guarantees stability if and only if $E^{n+1/2}$ is non-negative or, equivalently, if and only if the matrices $\left(\mathbf{I} - (\Delta t^2/4)\mathbf{A}_p\right)$ and $\mathbf{A}_p$ are both positive semidefinite. Hence, if $\lambda_{\min}$ and $\lambda_{\max}$ denote the smallest and largest eigenvalues of $\mathbf{A}_p$, respectively, the numerical scheme will be stable if and only if

$$0 \le \frac{\Delta t^2}{4}\lambda_{\min} \le \frac{\Delta t^2}{4}\lambda_{\max} \le 1.$$

For $p = 1$ we have $\mathbf{A}_p = \mathbf{A}$, and thus we recover the CFL condition of the standard leap-frog scheme

$$\Delta t \le \frac{2}{\sqrt{\lambda_{\max}}} = \Delta t_{LF}.$$

For $p > 1$, the matrix $\mathbf{A}_p$ explicitly depends on Δt, and so do its eigenvalues. Moreover, as the eigenvalues of $\mathbf{A}$ and $\mathbf{A}_p$ do not coincide, the analytical derivation of a sharp CFL condition is not obvious. In Section 6, we shall study the behavior of the eigenvalues of $(\Delta t^2/4)\mathbf{A}_p$ for an IP–DG discretisation of Maxwell's equations in two space dimensions. A more detailed numerical study of the eigenvalues of $(\Delta t^2/4)\mathbf{A}_p$ for the one-dimensional wave equation is presented in [25].

4.2. Local time-stepping method in a conducting medium

We shall now derive a second-order local time-stepping method for the semi-discrete Maxwell equations (5) in a general conducting medium with $\mathbf{D} \neq \mathbf{0}$. In contrast to the time-stepping scheme presented in Section 4.1 for the case $\mathbf{D} = \mathbf{0}$, which can be seen as a natural extension of [25] to the inhomogeneous case, we are now faced with several difficulties due to the additional $\mathbf{D}\mathbf{z}'(t)$ term. First, as in standard FD/FE–TD methods in conducting media [2,5], we shall treat that term implicitly to avoid any additional CFL restriction; else, the stability condition will be more restrictive than that with the non-dissipative scheme, depending on the magnitude of σ [23]. Nevertheless, the resulting scheme will be explicit, since $\mathbf{D}$ is essentially a diagonal matrix. Second, we can no longer take advantage of any inherent symmetry in time of the solution. Third, to avoid any loss of accuracy, we must carefully initialize the local time-stepping scheme, which again is based on the highly efficient (two-step) leap-frog method.

Lemma 4. *The exact solution* $\mathbf{z}(t)$ *of* (5) *satisfies*

$$\begin{aligned}&\mathbf{z}(t+\Delta t) - 2\mathbf{z}(t) + \mathbf{z}(t-\Delta t) + \frac{\Delta t}{2}\mathbf{D}\left(\mathbf{z}(t+\Delta t) - \mathbf{z}(t-\Delta t)\right)\\ &\quad = \Delta t^2 \int_{-1}^{1} (1-|\theta|)\left(\mathbf{R}(t+\theta\Delta t) - \mathbf{A}\mathbf{z}(t+\theta\Delta t)\right)\,\mathrm{d}\theta + \mathcal{O}(\Delta t^4).\end{aligned} \tag{29}$$

Proof. Since $\mathbf{z}(t)$ solves (5), we deduce from (7) that

$$\begin{aligned}\mathbf{z}(t+\Delta t) - 2\mathbf{z}(t) + \mathbf{z}(t-\Delta t) &= \Delta t^2 \int_{-1}^{1} (1-|\theta|)\left(\mathbf{R}(t+\theta\Delta t) - \mathbf{A}\mathbf{z}(t+\theta\Delta t)\right)\mathrm{d}\theta\\ &\quad - \Delta t^2 \mathbf{D}\int_{-1}^{1}(1-|\theta|)\frac{\mathrm{d}\mathbf{z}}{\mathrm{d}t}(t+\theta\Delta t)\,\mathrm{d}\theta.\end{aligned} \tag{30}$$

We now concentrate on the new term involving $\mathbf{z}'$ in (30). Integration by parts yields

$$\begin{aligned}\Delta t^2\mathbf{D}\int_{-1}^{1}(1-|\theta|)\mathbf{z}'(t+\theta\Delta t)\,\mathrm{d}\theta &= \Delta t\mathbf{D}\int_{t-\Delta t}^{t+\Delta t}\left(1 - \frac{|s-t|}{\Delta t}\right)\mathbf{z}'(s)\,\mathrm{d}s\\ &= \Delta t\mathbf{D}\left(-\mathbf{z}(t-\Delta t) + \int_{t-\Delta t}^{t}\frac{s-t}{\Delta t}\mathbf{z}'(s)\,\mathrm{d}s + \mathbf{z}(t+\Delta t) - \int_{t}^{t+\Delta t}\frac{s-t}{\Delta t}\mathbf{z}'(s)\,\mathrm{d}s\right)\\ &= \mathbf{D}\left(\int_{t}^{t+\Delta t}\mathbf{z}(s)\,\mathrm{d}s - \int_{t-\Delta t}^{t}\mathbf{z}(s)\,\mathrm{d}s\right).\end{aligned} \tag{31}$$

Let $g(s) = \mathbf{D}\mathbf{z}(s)$ in (31). We shall now show that

$$\int_t^{t+\Delta t} g(s)\,\mathrm{d}s - \int_{t-\Delta t}^{t} g(s)\,\mathrm{d}s = \frac{\Delta t}{2}\left(g(t+\Delta t) - g(t-\Delta t)\right) + \mathcal{O}(\Delta t^4).$$

By Taylor expansion and the mean value theorem, we find

$$\begin{aligned}\int_t^{t+\Delta t} g(s)\,\mathrm{d}s - \int_{t-\Delta t}^{t} g(s)\,\mathrm{d}s &= \Delta t^2 g'(t) + \int_t^{t+\Delta t} \frac{s^3}{6} g'''(\xi)\,\mathrm{d}s - \int_{t-\Delta t}^{t} \frac{s^3}{6} g'''(\xi)\,\mathrm{d}s \\ &= \Delta t^2 g'(t) + \frac{\Delta t^4}{24}\left(g'''(\eta_1) + g'''(\eta_2)\right),\end{aligned}$$

where $\eta_1 \in [t, t+\Delta t]$ and $\eta_2 \in [t-\Delta t, t]$. Replacing $g'(t)$ by second-order central finite differences, we thus obtain

$$\frac{\Delta t}{2}\left(g(t+\Delta t) - g(t-\Delta t)\right) - \left(\int_t^{t+\Delta t} g(s)\,\mathrm{d}s - \int_{t-\Delta t}^{t} g(s)\,\mathrm{d}s\right) = -\frac{\Delta t^4}{24}\left(g'''(\eta_1) + g'''(\eta_2)\right) + \mathcal{O}(\Delta t^4),$$

which completes the proof. □

To derive a second-order local time-stepping method for (5), we now split the vectors $\mathbf{z}(t)$ and $\mathbf{R}(t)$ as in (10) and approximate the integrands in (29) as follows:

$$\begin{aligned}&\mathbf{R}^{[\mathrm{coarse}]}(t+\theta\Delta t) + \mathbf{R}^{[\mathrm{fine}]}(t+\theta\Delta t) \simeq \mathbf{R}^{[\mathrm{coarse}]}(t) + \mathbf{P}\mathbf{R}(t+\theta\Delta t),\\ &\mathbf{A}\left(\mathbf{z}^{[\mathrm{coarse}]}(t+\theta\Delta t) + \mathbf{z}^{[\mathrm{fine}]}(t+\theta\Delta t)\right) \simeq \mathbf{A}\mathbf{z}^{[\mathrm{coarse}]}(t) + \mathbf{A}\mathbf{P}\mathbf{z}(\theta\Delta t).\end{aligned}$$

From Lemma 4 we thus have

$$\begin{aligned}&\mathbf{z}(t+\Delta t) - 2\mathbf{z}(t) + \mathbf{z}(t-\Delta t) + \frac{\Delta t}{2}\mathbf{D}\left(\mathbf{z}(t+\Delta t) - \mathbf{z}(t-\Delta t)\right)\\ &\quad\simeq \Delta t^2\left\{(\mathbf{I}-\mathbf{P})\mathbf{R}(t) - \mathbf{A}(\mathbf{I}-\mathbf{P})\mathbf{z}(t)\right\} + \Delta t^2\int_{-1}^{1}(1-|\theta|)\left\{\mathbf{P}\mathbf{R}(t+\theta\Delta t) - \mathbf{A}\mathbf{P}\mathbf{z}(\theta\Delta t)\right\}\,\mathrm{d}\theta.\end{aligned} \tag{32}$$

Next for fixed t, let $\widetilde{\mathbf{z}}(\tau)$ solve the differential equation

$$\begin{aligned}&\frac{\mathrm{d}^2\widetilde{\mathbf{z}}}{\mathrm{d}\tau^2}(\tau) + \mathbf{D}\frac{\mathrm{d}\widetilde{\mathbf{z}}}{\mathrm{d}\tau}(\tau) = (\mathbf{I}-\mathbf{P})\mathbf{R}(t) - \mathbf{A}(\mathbf{I}-\mathbf{P})\mathbf{z}(t) + \mathbf{P}\mathbf{R}(t+\tau) - \mathbf{A}\mathbf{P}\widetilde{\mathbf{z}}(\tau),\\ &\widetilde{\mathbf{z}}(0) = \mathbf{z}(t),\\ &\widetilde{\mathbf{z}}'(0) = \nu,\end{aligned} \tag{33}$$

where ν will be specified below. By applying Lemma 4 now to $\widetilde{\mathbf{z}}(t)$, we obtain

$$\begin{aligned}\widetilde{\mathbf{z}}(\Delta t) - 2\widetilde{\mathbf{z}}(0) + \widetilde{\mathbf{z}}(-\Delta t) + \frac{\Delta t}{2}\mathbf{D}\left(\widetilde{\mathbf{z}}(\Delta t) - \widetilde{\mathbf{z}}(-\Delta t)\right) &= \Delta t^2\left\{(\mathbf{I}-\mathbf{P})\mathbf{R}(t) - \mathbf{A}(\mathbf{I}-\mathbf{P})\mathbf{z}(t)\right\}\\ &\quad + \Delta t^2\int_{-1}^{1}(1-|\theta|)\left\{\mathbf{P}\mathbf{R}(t+\theta\Delta t) - \mathbf{A}\mathbf{P}\widetilde{\mathbf{z}}(\theta\Delta t)\right\}\,\mathrm{d}\theta.\end{aligned} \tag{34}$$

From the comparison of (32) and (34), we thus infer that

$$\mathbf{z}(t+\Delta t) + \mathbf{z}(t-\Delta t) + \frac{\Delta t}{2}\mathbf{D}\left(\mathbf{z}(t+\Delta t) - \mathbf{z}(t-\Delta t)\right) \simeq \widetilde{\mathbf{z}}(\Delta t) + \widetilde{\mathbf{z}}(-\Delta t) + \frac{\Delta t}{2}\mathbf{D}\left(\widetilde{\mathbf{z}}(\Delta t) - \widetilde{\mathbf{z}}(-\Delta t)\right). \tag{35}$$

In our local time-stepping scheme, we shall use the right side of (35) to approximate the left side. In doing so, we must carefully choose ν in (33) to minimize that approximation error. By using Taylor expansions and the fact that $\mathbf{z}$ and $\widetilde{\mathbf{z}}$ solve (5) and (33), respectively, we obtain

$$\begin{aligned}&\mathbf{z}(t+\Delta t) + \mathbf{z}(t-\Delta t) = 2\mathbf{z}(t) + \mathbf{z}''(t)\Delta t^2 + \mathcal{O}(\Delta t^4) = 2\mathbf{z}(t) + (\mathbf{R}(t) - \mathbf{A}\mathbf{z}(t) - \mathbf{D}\mathbf{z}'(t))\Delta t^2 + \mathcal{O}(\Delta t^4),\\ &\widetilde{\mathbf{z}}(\Delta t) + \widetilde{\mathbf{z}}(-\Delta t) = 2\widetilde{\mathbf{z}}(0) + \widetilde{\mathbf{z}}''(0)\Delta t^2 + \mathcal{O}(\Delta t^4) = 2\mathbf{z}(t) + (\mathbf{R}(t) - \mathbf{A}\mathbf{z}(t) - \mathbf{D}\nu)\Delta t^2 + \mathcal{O}(\Delta t^4),\end{aligned}$$

together with

$$\begin{aligned}&\mathbf{z}(t+\Delta t) - \mathbf{z}(t-\Delta t) = 2\mathbf{z}'(t)\Delta t + \mathcal{O}(\Delta t^3),\\ &\widetilde{\mathbf{z}}(\Delta t) - \widetilde{\mathbf{z}}(-\Delta t) = 2\nu\Delta t + \mathcal{O}(\Delta t^3).\end{aligned}$$

Hence for arbitrary ν, the right side of (35) is not sufficiently accurate to approximate the left side while preserving overall second-order accuracy. However, if we choose

$$\nu = \mathbf{z}'(t)$$

in (33), the $\mathcal{O}(\Delta t^2)$ terms in (35) cancel each other and overall second-order accuracy of the scheme can be achieved. Since the term on the right side of (35) is not symmetric in time, unlike in the previous section (see (15) and (17)), we need to compute the value of $\widetilde{\mathbf{z}}(\tau)$ both at $\tau = \Delta t$ and at $\tau = -\Delta t$. Clearly, in doing so we must also ensure that the overall numerical scheme remains second-order accurate in time, as we show below.

For the numerical solution of (33), we shall use the leap-frog scheme with the local time-step $\Delta\tau = \Delta t/p$. Since the leap-frog scheme is a two-step method, we need a second-order approximation of $\widetilde{\mathbf{z}}'(0) = \mathbf{z}'(t)$ during every initial local time-step. Since the value of $\mathbf{z}_{n+1}$ is still unknown at time $t = t_n$, we now derive a second-order approximation $\mathbf{z}'_n \simeq \mathbf{z}'(t)$ that uses only $\mathbf{z}_n$ and $\mathbf{z}_{n-1}$. First, we approximate

$$\mathbf{z}'_n \simeq \frac{\mathbf{z}'_{n-1/2} + \mathbf{z}'_{n+1/2}}{2}, \tag{36}$$

where both $\mathbf{z}'_{n-1/2} \simeq \mathbf{z}'(t - \Delta t/2)$ and $\mathbf{z}'_{n+1/2} \simeq \mathbf{z}'(t + \Delta t/2)$ are second-order approximations. By using second-order central differences for $\mathbf{z}'_{n-1/2}$,

$$\mathbf{z}'_{n-1/2} = \frac{\mathbf{z}_n - \mathbf{z}_{n-1}}{\Delta t} + \mathcal{O}(\Delta t^2), \tag{37}$$

and the differential equation (5) for $\mathbf{z}'_{n+1/2}$,

$$\frac{\mathbf{z}'_{n+1/2} - \mathbf{z}'_{n-1/2}}{\Delta t} + \mathbf{D}\mathbf{z}'_n = \mathbf{R}_n - \mathbf{A}\mathbf{z}_n + \mathcal{O}(\Delta t^2),$$

we obtain

$$\mathbf{z}'_{n+1/2} = \left(\mathbf{I} + \frac{\Delta t}{2}\mathbf{D}\right)^{-1} \left\{\left(\mathbf{I} - \frac{\Delta t}{2}\mathbf{D}\right)\frac{\mathbf{z}_n - \mathbf{z}_{n-1}}{\Delta t} + \Delta t\mathbf{R}_n - \Delta t\mathbf{A}\mathbf{z}_n\right\} + \mathcal{O}(\Delta t^2). \tag{38}$$

Then, we insert (37), (38) into (36), which yields a second-order approximation of $\mathbf{z}'(t)$.

In summary, the second-order local time-stepping algorithm for the solution of (5) computes $\mathbf{z}_{n+1} \simeq \mathbf{z}(t + \Delta t)$, for given $\mathbf{z}_n$ and $\mathbf{z}_{n-1}$, as follows:

Algorithm 2. 1. Set $\mathbf{w} := (\mathbf{I} - \mathbf{P})\mathbf{R}_n - \mathbf{A}(\mathbf{I} - \mathbf{P})\mathbf{z}_n$, $\widetilde{\mathbf{z}}_0 := \mathbf{z}_n$ and

$$\mathbf{z}'_n := \frac{1}{2}\left[\frac{\mathbf{z}_n - \mathbf{z}_{n-1}}{\Delta t} + \left(\mathbf{I} + \frac{\Delta t}{2}\mathbf{D}\right)^{-1}\left\{\left(\mathbf{I} - \frac{\Delta t}{2}\mathbf{D}\right)\frac{\mathbf{z}_n - \mathbf{z}_{n-1}}{\Delta t} + \Delta t\mathbf{R}_n - \Delta t\mathbf{A}\mathbf{z}_n\right\}\right].$$

2. Compute

$$\widetilde{\mathbf{z}}_{1/p} := \widetilde{\mathbf{z}}_0 + \frac{\Delta t}{p}\mathbf{z}'_n + \frac{1}{2}\left(\frac{\Delta t}{p}\right)^2\left(\mathbf{w} + \mathbf{P}\mathbf{R}_{n,0} - \mathbf{A}\mathbf{P}\widetilde{\mathbf{z}}_0 - \mathbf{D}\mathbf{z}'_n\right) \quad \text{and}$$

$$\widetilde{\mathbf{z}}_{-1/p} := \widetilde{\mathbf{z}}_0 - \frac{\Delta t}{p}\mathbf{z}'_n + \frac{1}{2}\left(\frac{\Delta t}{p}\right)^2\left(\mathbf{w} + \mathbf{P}\mathbf{R}_{n,0} - \mathbf{A}\mathbf{P}\widetilde{\mathbf{z}}_0 - \mathbf{D}\mathbf{z}'_n\right).$$

3. For $m = 1, \ldots, p-1$, compute

$$\widetilde{\mathbf{z}}_{(m+1)/p} := \left(\mathbf{I} + \frac{\Delta t}{2p}\mathbf{D}\right)^{-1}\left\{2\widetilde{\mathbf{z}}_{m/p} - \left(\mathbf{I} - \frac{\Delta t}{2p}\mathbf{D}\right)\widetilde{\mathbf{z}}_{(m-1)/p} + \left(\frac{\Delta t}{p}\right)^2(\mathbf{w} + \mathbf{P}\mathbf{R}_{n,m} - \mathbf{A}\mathbf{P}\widetilde{\mathbf{z}}_{m/p})\right\}$$

and

$$\widetilde{\mathbf{z}}_{-(m+1)/p} := \left(\mathbf{I} - \frac{\Delta t}{2p}\mathbf{D}\right)^{-1}\left\{2\widetilde{\mathbf{z}}_{-m/p} - \left(\mathbf{I} + \frac{\Delta t}{2p}\mathbf{D}\right)\widetilde{\mathbf{z}}_{-(m-1)/p} + \left(\frac{\Delta t}{p}\right)^2(\mathbf{w} + \mathbf{P}\mathbf{R}_{n,-m} - \mathbf{A}\mathbf{P}\widetilde{\mathbf{z}}_{-m/p})\right\}.$$

4. Compute

$$\mathbf{z}_{n+1} := \widetilde{\mathbf{z}}_1 + \left(\mathbf{I} + \frac{\Delta t}{2}\mathbf{D}\right)^{-1}\left(\mathbf{I} - \frac{\Delta t}{2}\mathbf{D}\right)(-\mathbf{z}_{n-1} + \widetilde{\mathbf{z}}_{-1}).$$

Here, we have used the same notations as in Algorithm 1. If ε and σ are piecewise constant in each element, $\mathbf{M}_\varepsilon$ and $\mathbf{M}_\sigma$ can be diagonalised simultaneously and hence the matrix $\mathbf{D}$ is diagonal. If ε and σ vary in elements, $\mathbf{D}$ is a block-diagonal matrix and both $(\mathbf{I} \pm (\Delta t/2p)\mathbf{D})$ and $(\mathbf{I} \pm (\Delta t/2)\mathbf{D})$ can be explicitly inverted at low cost. In that sense, the local time-stepping scheme (Algorithm 2) is truly explicit. Again, if the fraction of nonzero entries in $\mathbf{P}$ is small, the overall cost is dominated by the computation of $\mathbf{w}$ in step 1.

We now establish the accuracy of the above local time-stepping scheme. For simplicity, we restrict ourselves to the case $p = 2$, as the extension to the general case $p > 2$ is straightforward but cumbersome.

Proposition 4. *For $\mathbf{R}(t) \in C^2([0,T])$, the local time-stepping method (Algorithm 2) is second-order accurate.*

Proof. Recall that

$$\left(\mathbf{I}+\frac{\Delta t}{2}\mathbf{D}\right)\mathbf{z}_{n+1} = \left(\mathbf{I}+\frac{\Delta t}{2}\mathbf{D}\right)\widetilde{\mathbf{z}}_1 - \left(\mathbf{I}-\frac{\Delta t}{2}\mathbf{D}\right)\mathbf{z}_{n-1} + \left(\mathbf{I}-\frac{\Delta t}{2}\mathbf{D}\right)\widetilde{\mathbf{z}}_{-1}. \tag{39}$$

We shall now show that

$$\left(\mathbf{I}+\frac{\Delta t}{2}\mathbf{D}\right)\widetilde{\mathbf{z}}_1 + \left(\mathbf{I}-\frac{\Delta t}{2}\mathbf{D}\right)\widetilde{\mathbf{z}}_{-1} = 2\mathbf{z}_n + \Delta t^2(\mathbf{R}_{n,0} - \mathbf{A}\mathbf{z}_n) + \mathcal{O}(\Delta t^4) \tag{40}$$

holds. To do so, let

$$\widetilde{Z}_1 = 2\widetilde{\mathbf{z}}_{1/2} - \left(\mathbf{I}-\frac{\Delta t}{4}\mathbf{D}\right)\widetilde{\mathbf{z}}_0 + \left(\frac{\Delta t}{2}\right)^2(\mathbf{w} + \mathbf{P}\mathbf{R}_{n,1} - \mathbf{A}\mathbf{P}\widetilde{\mathbf{z}}_{1/2}),$$

$$\widetilde{Z}_{-1} = 2\widetilde{\mathbf{z}}_{-1/2} - \left(\mathbf{I}+\frac{\Delta t}{4}\mathbf{D}\right)\widetilde{\mathbf{z}}_0 + \left(\frac{\Delta t}{2}\right)^2(\mathbf{w} + \mathbf{P}\mathbf{R}_{n,-1} - \mathbf{A}\mathbf{P}\widetilde{\mathbf{z}}_{-1/2}).$$

Then,

$$\left(\mathbf{I}+\frac{\Delta t}{2}\mathbf{D}\right)\widetilde{\mathbf{z}}_1 + \left(\mathbf{I}-\frac{\Delta t}{2}\mathbf{D}\right)\widetilde{\mathbf{z}}_{-1} = \left(\mathbf{I}+\frac{\Delta t}{2}\mathbf{D}\right)\left(\mathbf{I}+\frac{\Delta t}{4}\mathbf{D}\right)^{-1}\widetilde{Z}_1 + \left(\mathbf{I}-\frac{\Delta t}{2}\mathbf{D}\right)\left(\mathbf{I}-\frac{\Delta t}{4}\mathbf{D}\right)^{-1}\widetilde{Z}_{-1}. \tag{41}$$

Next, we recall that $\mathbf{D} = \mathbf{M}_\varepsilon^{-\frac{1}{2}}\mathbf{M}_\sigma\mathbf{M}_\varepsilon^{-\frac{1}{2}}$, where $\mathbf{M}_\varepsilon$, $\mathbf{M}_\sigma$ denote the mass matrices with weights ε, σ, respectively. Since $\varepsilon(\mathbf{x}) \geq \varepsilon_0 > 0$, we have $\|\mathbf{D}\| < C$, with C independent of the mesh size h. For sufficiently small Δt, we have $(\Delta t/4)\,\|\mathbf{D}\| < 1$ independently of h. Then, we may use the expansion

$$\left(\mathbf{I} \pm \frac{\Delta t}{4}\mathbf{D}\right)^{-1} = \mathbf{I} \mp \frac{\Delta t}{4}\mathbf{D} + \frac{\Delta t^2}{16}\mathbf{D}^2 \mp \frac{\Delta t^3}{64}\mathbf{D}^3 + \mathcal{O}(\Delta t^4). \tag{42}$$

Inserting (42) into (41), we find

$$\begin{aligned}\left(\mathbf{I}+\frac{\Delta t}{2}\mathbf{D}\right)\widetilde{\mathbf{z}}_1 + \left(\mathbf{I}-\frac{\Delta t}{2}\mathbf{D}\right)\widetilde{\mathbf{z}}_{-1} &= (\widetilde{Z}_1 + \widetilde{Z}_{-1}) + \frac{\Delta t}{4}(\widetilde{Z}_1 - \widetilde{Z}_{-1}) - \frac{\Delta t^2}{16}(\widetilde{Z}_1 + \widetilde{Z}_{-1}) \\ &\quad - \frac{\Delta t^3}{64}(\widetilde{Z}_1 - \widetilde{Z}_{-1}) + \mathcal{O}(\Delta t^4).\end{aligned} \tag{43}$$

Next, we derive explicit expressions for $\widetilde{Z}_1$ and $\widetilde{Z}_{-1}$. By using (42) we first rewrite $\mathbf{z}_n'$ as

$$\mathbf{z}_n' = \frac{1}{2\Delta t}(\mathbf{z}_n - \mathbf{z}_{n-1})T_1 + \frac{\Delta t}{2}\left(\mathbf{I}-\frac{\Delta t}{2}\mathbf{D}\right)(\mathbf{R}_{n,0} - \mathbf{A}\mathbf{z}_n) + \mathcal{O}(\Delta t^3),$$

with $T_1 := \mathbf{I} + \left(\mathbf{I} - \frac{\Delta t}{2}\mathbf{D}\right)^2 + \mathcal{O}(\Delta t^2)$ and insert it into $\widetilde{\mathbf{z}}_{1/2}$ and $\widetilde{\mathbf{z}}_{-1/2}$. Thus, we obtain

$$\begin{aligned}\widetilde{\mathbf{z}}_{1/2} &= \mathbf{z}_n + \frac{1}{4}(\mathbf{z}_n - \mathbf{z}_{n-1})T_1 - \frac{\Delta t}{16}(\mathbf{z}_n - \mathbf{z}_{n-1})\mathbf{D}T_1 + \frac{\Delta t^2}{8}(\mathbf{R}_{n,0} - \mathbf{A}\mathbf{z}_n) + \frac{\Delta t^2}{4}(\mathbf{R}_{n,0} - \mathbf{A}\mathbf{z}_n)\left(\mathbf{I}-\frac{\Delta t}{2}\mathbf{D}\right) \\ &\quad - \frac{\Delta t^3}{16}(\mathbf{R}_{n,0} - \mathbf{A}\mathbf{z}_n)\mathbf{D}\left(\mathbf{I}-\frac{\Delta t}{2}\mathbf{D}\right) + \mathcal{O}(\Delta t^4),\end{aligned}$$

and similarly for $\widetilde{\mathbf{z}}_{-1/2}$. By rearranging terms we then rewrite $\widetilde{Z}_1$ and $\widetilde{Z}_{-1}$ as

$$\begin{aligned}\widetilde{Z}_1 &= \mathbf{z}_n + \frac{1}{2}(\mathbf{z}_n - \mathbf{z}_{n-1})T_1 + \frac{\Delta t}{4}\mathbf{D}\mathbf{z}_n - \frac{\Delta t}{8}(\mathbf{z}_n - \mathbf{z}_{n-1})\mathbf{D}T_1 - \frac{\Delta t^2}{16}(\mathbf{z}_n - \mathbf{z}_{n-1})\mathbf{A}\mathbf{P}T_1 + \frac{\Delta t^2}{2}(\mathbf{R}_{n,0} - \mathbf{A}\mathbf{z}_n) \\ &\quad + \frac{\Delta t^2}{2}(\mathbf{R}_{n,0} - \mathbf{A}\mathbf{z}_n)\left(\mathbf{I}-\frac{\Delta t}{2}\mathbf{D}\right) + \frac{\Delta t^2}{4}(\mathbf{P}\mathbf{R}_{n,1} - \mathbf{P}\mathbf{R}_{n,0}) - \frac{\Delta t^3}{8}(\mathbf{R}_{n,0} - \mathbf{A}\mathbf{z}_n)\mathbf{D}\left(\mathbf{I}-\frac{\Delta t}{2}\mathbf{D}\right) + \mathcal{O}(\Delta t^4), \\ \widetilde{Z}_{-1} &= \mathbf{z}_n - \frac{1}{2}(\mathbf{z}_n - \mathbf{z}_{n-1})T_1 - \frac{\Delta t}{4}\mathbf{D}\mathbf{z}_n - \frac{\Delta t}{8}(\mathbf{z}_n - \mathbf{z}_{n-1})\mathbf{D}T_1 + \frac{\Delta t^2}{16}(\mathbf{z}_n - \mathbf{z}_{n-1})\mathbf{A}\mathbf{P}T_1 + \frac{\Delta t^2}{2}(\mathbf{R}_{n,0} - \mathbf{A}\mathbf{z}_n) \\ &\quad - \frac{\Delta t^2}{2}(\mathbf{R}_{n,0} - \mathbf{A}\mathbf{z}_n)\left(\mathbf{I}-\frac{\Delta t}{2}\mathbf{D}\right) + \frac{\Delta t^2}{4}(\mathbf{P}\mathbf{R}_{n,-1} - \mathbf{P}\mathbf{R}_{n,0}) - \frac{\Delta t^3}{8}(\mathbf{R}_{n,0} - \mathbf{A}\mathbf{z}_n)\mathbf{D}\left(\mathbf{I}-\frac{\Delta t}{2}\mathbf{D}\right) + \mathcal{O}(\Delta t^4).\end{aligned}$$

After inserting the resulting expressions for $\widetilde{Z}_1$ and $\widetilde{Z}_{-1}$ into (43) and further simplifications, we obtain (40).

Finally, we insert (40) into (39) to find

$$\left(\mathbf{I}+\frac{\Delta t}{2}\mathbf{D}\right)\mathbf{z}_{n+1} = -\left(\mathbf{I}-\frac{\Delta t}{2}\mathbf{D}\right)\mathbf{z}_{n-1} + 2\mathbf{z}_n + \Delta t^2(\mathbf{R}_{n,0} - \mathbf{A}\mathbf{z}_n) + \mathcal{O}(\Delta t^4), \tag{44}$$

which is equivalent to

$$\frac{\mathbf{z}_{n+1} - 2\mathbf{z}_n + \mathbf{z}_{n-1}}{\Delta t^2} + \mathbf{D}\frac{\mathbf{z}_{n+1} - \mathbf{z}_{n-1}}{2\Delta t} + \mathbf{A}\mathbf{z}_n = \mathbf{R}_{n,0} + \mathcal{O}\left(\Delta t^2\right).$$

From the comparison with (5) we conclude that the local time-stepping scheme is second-order accurate. □

Remark 2. For $\sigma = 0$ ($\mathbf{D} = \mathbf{0}$), Algorithm 2 coincides with Algorithm 1 and thus also conserves the discrete energy (28). For $\sigma \neq 0$ and $p = 1$, i.e. no local mesh refinement, one can easily show that the energy is no longer conserved but decays with time (independently of σ) under the same CFL condition as in the case with $\sigma = 0$.

5. High-order explicit local time-stepping

In a non-conducting medium, Maxwell's equations correspond to a separable Hamiltonian system. This fact explains the success of symplectic integrators, such as the leap-frog (or Störmer–Verlet) method, when combined with a symmetric discretisation in space based on centred finite differences or centred DG fluxes, for instance. Indeed the fully discrete numerical scheme will then conserve (a discrete version of) the energy, too. Clearly, standard symplectic partitioned Runge–Kutta (Lobatto IIIA–IIIB pairs) or composition methods [31] can be used to achieve higher accuracy [32]. Because the Hamiltonian here is separable, those higher order versions will also remain explicit in time, like the Störmer–Verlet method. Since Maxwell's equations are linear, we instead opt for the even more efficient modified equation (ME) approach [33] in Section 5, which leads to explicit local-time stepping of arbitrarily high (even) order. In a conducting medium, however, Maxwell's equations are dissipative and those approaches no longer yield explicit high-order time-marching schemes. Thus standard explicit Runge–Kutta or multi-step methods become the methods of choice [13,21,34]. The development of explicit local time-stepping schemes of arbitrarily high accuracy based on RK methods is a topic of active research while an explicit stability criterion still remains an open problem.

5.1. Modified equation approach

Following the ME approach, we replace $\mathbf{A}\mathbf{z}(t+\theta\Delta t)$ in (8) by its Taylor expansion

$$\mathbf{A}\mathbf{z}(t+\theta\Delta t) = \mathbf{A}\left(\mathbf{z}(t) + \theta\Delta t\mathbf{z}'(t) + \frac{\theta^2\Delta t^2}{2}\mathbf{z}''(t) + \frac{\theta^3\Delta t^3}{6}\mathbf{z}'''(t)\right) + \mathcal{O}(\Delta t^4).$$

Then, the integrals involving odd powers of θ vanish. Next, by using that $\mathbf{z}''(t) = \mathbf{R}(t) - \mathbf{A}\mathbf{z}(t)$ and the Simpson quadrature rule for the term that involves $\mathbf{R}(t+\theta\Delta t)$, we obtain the fourth-order modified equation scheme.

$$\frac{\mathbf{z}_{m+1} - 2\mathbf{z}_m + \mathbf{z}_{m-1}}{\Delta t^2} = \mathbf{R}_m - \mathbf{A}\mathbf{z}_m + \frac{\Delta t^2}{12}\mathbf{A}^2\mathbf{z}_m - \frac{\Delta t^2}{12}\mathbf{A}\mathbf{R}_m + \frac{1}{3}\left(\mathbf{R}_{m-1/2} - 2\mathbf{R}_m + \mathbf{R}_{m+1/2}\right) + \mathcal{O}(\Delta t^4), \tag{45}$$

where $\mathbf{z}_m \simeq \mathbf{z}(t_m)$, $\mathbf{R}_m \simeq \mathbf{R}(t_m)$ and $\mathbf{R}_{m\pm1/2} \simeq \mathbf{R}(t_m \pm \Delta t/2)$. Clearly, integration schemes of arbitrary (even) order can be obtained by using additional terms in the Taylor expansion. Since the maximal time-step allowed by the fourth-order ME method is about 70% times *larger* than that of the leap-frog scheme [35], the additional work needed for the improved accuracy is quite small; hence, the ME method is extremely efficient.

5.2. Fourth-order local time-stepping method in a non-conducting medium

We now derive a fourth-order local time-stepping method for (6). Similarly to the derivation in Section 4.1, we split the vectors $\mathbf{z}(t)$ and $\mathbf{R}(t)$ in (11) into a fine and a coarse part, and shall treat $\mathbf{z}^{[\text{fine}]}(t)$ and $\mathbf{R}^{[\text{fine}]}(t)$ differently from $\mathbf{z}^{[\text{coarse}]}(t)$ and $\mathbf{R}^{[\text{coarse}]}(t)$. We expand $\mathbf{z}^{[\text{coarse}]}(t+\theta\Delta t)$ in Taylor series as

$$\mathbf{z}^{[\text{coarse}]}(t+\theta\Delta t) = \mathbf{z}^{[\text{coarse}]}(t) + \theta\Delta t\frac{\mathrm{d}\mathbf{z}^{[\text{coarse}]}}{\mathrm{d}t}(t) + \frac{\theta^2\Delta t^2}{2}\frac{\mathrm{d}^2\mathbf{z}^{[\text{coarse}]}}{\mathrm{d}t^2}(t) + \frac{\theta^3\Delta t^3}{6}\frac{\mathrm{d}^3\mathbf{z}^{[\text{coarse}]}}{\mathrm{d}t^3}(t) + \mathcal{O}(\Delta t^4)$$

and insert it into (11). In (11), the integrals involving odd powers of θ vanish. By using

$$\frac{\mathrm{d}^2\mathbf{z}^{[\text{coarse}]}}{\mathrm{d}t^2}(t) = (\mathbf{I}-\mathbf{P})\frac{\mathrm{d}^2\mathbf{z}}{\mathrm{d}t^2}(t) = (\mathbf{I}-\mathbf{P})\mathbf{R}(t) - (\mathbf{I}-\mathbf{P})\mathbf{A}\mathbf{z}(t)$$

and the Simpson quadrature rule for the term in (11) that involves $\mathbf{R}^{[\mathrm{coarse}]}(t+\theta\Delta t)$, we find that

$$\begin{aligned}\mathbf{z}(t+\Delta t)-2\mathbf{z}(t)+\mathbf{z}(t-\Delta t) &= \Delta t^2\{(\mathbf{I}-\mathbf{P})\mathbf{R}(t)-\mathbf{A}(\mathbf{I}-\mathbf{P})\mathbf{z}(t)\}+\frac{\Delta t^4}{12}\mathbf{A}(\mathbf{I}-\mathbf{P})\mathbf{A}\mathbf{z}(t)-\frac{\Delta t^4}{12}\mathbf{A}(\mathbf{I}-\mathbf{P})\mathbf{R}(t)\\ &\quad+\frac{\Delta t^2}{3}(\mathbf{I}-\mathbf{P})\left\{\mathbf{R}\left(t-\frac{\Delta t}{2}\right)-2\mathbf{R}(t)+\mathbf{R}\left(t+\frac{\Delta t}{2}\right)\right\}\\ &\quad+\Delta t^2\int_{-1}^{1}(1-|\theta|)\left\{\mathbf{R}^{[\mathrm{fine}]}(t+\theta\Delta t)-\mathbf{A}\mathbf{z}^{[\mathrm{fine}]}(t+\theta\Delta t)\right\}\,\mathrm{d}\theta. \qquad (46)\end{aligned}$$

Hence, if $\mathbf{P}=\mathbf{0}$ we recover the standard modified equation scheme (45).

Similarly to Section 4.1, we now approximate the right-hand side of (46) by solving the following differential equation for $\widetilde{\mathbf{z}}(\tau)$

$$\begin{aligned}\frac{\mathrm{d}^2\widetilde{\mathbf{z}}}{\mathrm{d}\tau^2}(\tau) &= (\mathbf{I}-\mathbf{P})\mathbf{R}(t)-\mathbf{A}(\mathbf{I}-\mathbf{P})\mathbf{z}(t)+\frac{1}{3}(\mathbf{I}-\mathbf{P})\left\{\mathbf{R}\left(t-\frac{\Delta t}{2}\right)-2\mathbf{R}(t)+\mathbf{R}\left(t+\frac{\Delta t}{2}\right)\right\}\\ &\quad+\frac{\tau^2}{2}\mathbf{A}(\mathbf{I}-\mathbf{P})\mathbf{A}\mathbf{z}(t)-\frac{\tau^2}{2}\mathbf{A}(\mathbf{I}-\mathbf{P})\mathbf{R}(t)+\mathbf{P}\mathbf{R}(t+\tau)-\mathbf{A}\mathbf{P}\widetilde{\mathbf{z}}(\tau),\\ \widetilde{\mathbf{z}}(0) &= \mathbf{z}(t),\\ \widetilde{\mathbf{z}}'(0) &= \nu,\end{aligned}$$

where ν will be specified below. Again, using Taylor expansions, we infer that

$$\mathbf{z}(t+\Delta t)+\mathbf{z}(t-\Delta t)=\widetilde{\mathbf{z}}(\Delta t)+\widetilde{\mathbf{z}}(-\Delta t)+\mathcal{O}(\Delta t^6).$$

Again, the quantity $\widetilde{\mathbf{z}}(\Delta t)+\widetilde{\mathbf{z}}(-\Delta t)$ does not depend on the value of ν, which we set to zero. As in Section 4.1, we set $\mathbf{q}(\tau):=\widetilde{\mathbf{z}}(\tau)+\widetilde{\mathbf{z}}(-\tau)$, which solves the differential equation

$$\begin{aligned}\frac{\mathrm{d}^2\mathbf{q}}{\mathrm{d}\tau^2}(\tau) &= 2\{(\mathbf{I}-\mathbf{P})\mathbf{R}(t)-\mathbf{A}(\mathbf{I}-\mathbf{P})\mathbf{z}(t)\}+\frac{2}{3}(\mathbf{I}-\mathbf{P})\left\{\mathbf{R}\left(t-\frac{\Delta t}{2}\right)-2\mathbf{R}(t)+\mathbf{R}\left(t+\frac{\Delta t}{2}\right)\right\}\\ &\quad+\tau^2\mathbf{A}(\mathbf{I}-\mathbf{P})\mathbf{A}\mathbf{z}(t)-\tau^2\mathbf{A}(\mathbf{I}-\mathbf{P})\mathbf{R}(t)+\mathbf{P}\{\mathbf{R}(t+\tau)+\mathbf{R}(t-\tau)\}-\mathbf{A}\mathbf{P}\mathbf{q}(\tau), \qquad (47)\\ \mathbf{q}(0) &= 2\mathbf{z}(t),\\ \mathbf{q}'(0) &= 0.\end{aligned}$$

Thus, we have

$$\mathbf{z}(t+\Delta t)+\mathbf{z}(t-\Delta t)=\mathbf{q}(\Delta t)+\mathcal{O}(\Delta t^6). \qquad (48)$$

Now, we approximate the right side of (8) by solving (47) with the fourth-order ME method on $[0,\Delta t]$ with a smaller time step $\Delta\tau=\Delta t/p$, and then use (48) to compute $\mathbf{z}(t+\Delta t)$.

In summary, the fourth-order algorithm for the solution of (6) computes $\mathbf{z}_{n+1}\simeq\mathbf{z}(t+\Delta t)$, given $\mathbf{z}_n$ and $\mathbf{z}_{n-1}$, as follows:

Algorithm 3. 1. Set $\mathbf{q}_0:=2\mathbf{z}_n$, $w_1:=(\mathbf{I}-\mathbf{P})\mathbf{R}_n-\mathbf{A}(\mathbf{I}-\mathbf{P})\mathbf{z}_n$, $w_2:=\mathbf{A}(\mathbf{I}-\mathbf{P})\mathbf{A}\mathbf{z}_n-\mathbf{A}(\mathbf{I}-\mathbf{P})\mathbf{R}_n$ and $r_1:=\mathbf{R}_{n-1/2}-2\mathbf{R}_n+\mathbf{R}_{n+1/2}$.
2. Compute

$$\begin{aligned}u &:= 2w_1+\frac{2}{3}(\mathbf{I}-\mathbf{P})r_1+2\mathbf{R}_{n,0}-\mathbf{A}\mathbf{P}\mathbf{q}_0\\ \mathbf{q}_{1/p} &:= \mathbf{q}_0+\frac{1}{2}\left(\frac{\Delta t}{p}\right)^2u+\frac{1}{24}\left(\frac{\Delta t}{p}\right)^4(2w_2+2\mathbf{P}r_1-\mathbf{A}\mathbf{P}u).\end{aligned}$$

3. For $m=1,\ldots,p-1$, compute

$$\begin{aligned}u_1 &:= 2w_1+\frac{2}{3}(\mathbf{I}-\mathbf{P})r_1+\left(\frac{m\Delta t}{p}\right)^2w_2+\mathbf{P}\left(\mathbf{R}_{n,m}+\mathbf{R}_{n,-m}\right)-\mathbf{A}\mathbf{P}\mathbf{q}_{m/p},\\ r &:= \mathbf{R}_{n,m-1/2}-2\mathbf{R}_{n,m}+\mathbf{R}_{n,m+1/2}+\mathbf{R}_{n,-m-1/2}-2\mathbf{R}_{n,-m}+\mathbf{R}_{n,-m+1/2},\\ u_2 &:= 2w_2+\mathbf{P}r-\mathbf{A}\mathbf{P}u_1,\\ \mathbf{q}_{(m+1)/p} &:= 2\mathbf{q}_{m/p}-\mathbf{q}_{(m-1)/p}+\left(\frac{\Delta t}{p}\right)^2u_1+\frac{1}{2}\left(\frac{\Delta t}{p}\right)^4u_2.\end{aligned}$$

4. Compute $\mathbf{z}_{n+1}:=-\mathbf{z}_{n-1}+\mathbf{q}_1$.

Here, Steps 1–3 correspond to the numerical solution of (47) until $\tau=\Delta t$ with the ME approach using the local time-step $\Delta\tau=\Delta t/p$. This algorithm requires three – two, without sources – multiplications by $\mathbf{A}(\mathbf{I}-\mathbf{P})$ and $2p$ further multiplications by $\mathbf{AP}$. For $\mathbf{P}=\mathbf{0}$, that is without any local time-stepping, Algorithm 3 reduces to the modified equation scheme (45) above. To establish the accuracy and stability of the above local time-stepping scheme, one must rewrite it in "leap-frog manner" following the approach in [25] for the homogeneous case and use extensions of Lemmas 1 and 2 (Section 4.1).

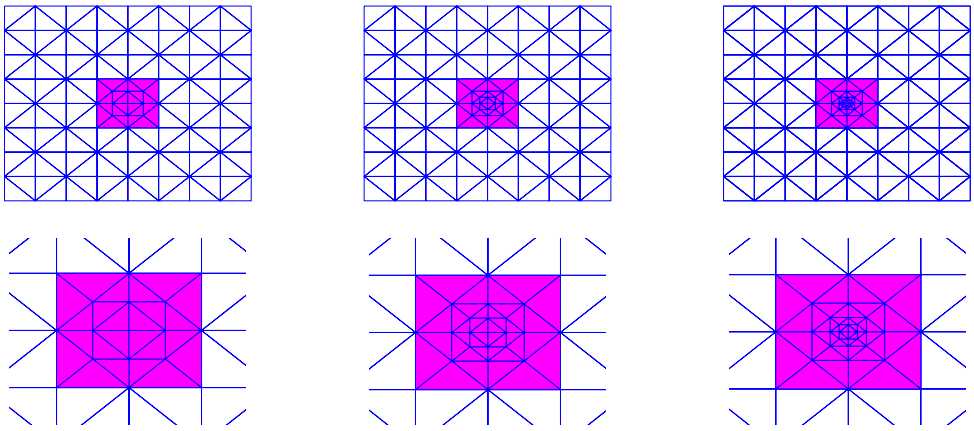

Fig. 1. The triangular meshes on (global) refinement level 1: local refinement with $p = 2$ (left), $p = 4$ (centre), and $p = 8$ (right). The darker triangles belong to the "fine" mesh and the lighter triangles to the "coarse" mesh.

6. Numerical experiments

We shall now present three numerical experiments to validate the theoretical results obtained for the local time-stepping methods and illustrate their usefulness in the presence of complex geometry. Throughout this section we use the IP–DG discretisation from Section 3 with linear triangular elements and fix the penalty parameter in (3) to $\alpha = 10$, for simplicity. First, we consider a model problem in a non-conducting source-free medium, for which the analytical solution is known. Here, we shall verify space–time second-order convergence and conservation of energy for different rates of local refinement, p. Moreover, we shall study the stability condition on the time step, Δt, for varying p, both for regular and unstructured triangulations. Second, we include an inhomogeneous source and verify the expected rates of convergence both in a conducting and in a non-conducting medium. Third, we illustrate the versatility of our local time-stepping schemes by simulating a Gaussian beam penetrating a cavity with a small hole embedded in a locally refined mesh.

6.1. Homogeneous source and non-conducting medium

We consider (1) in a non-conducting medium, i.e. $\sigma = 0$ throughout $\Omega = (-\pi, \pi)^2$, with $T = 2\pi$, $\mathbf{f} = \mathbf{0}$, and constant material parameters $\varepsilon = \mu = 1$. Furthermore, we set the initial conditions such that the solution corresponds to

$$\mathbf{u}(x, y, t) = \cos(t) \begin{pmatrix} \sin(y) \\ \sin(x) \end{pmatrix}.$$

The computational domain Ω is discretized with a regular triangular mesh of size $h^{\text{coarse}} = 0.23$. Then, we refine by a factor $p = 2, 4$ or 8 a square-shaped subregion of diagonal 1.4 at the centre of Ω; hence, $h^{\text{fine}} = h^{\text{coarse}}/p$. The fine mesh, that is the subregion of Ω where local time steps are required, then consists of all triangles of size $h_K < h^{\text{coarse}}$, as indicated in Fig. 1.

For every time-step Δt, we shall take p local time-steps of size $\Delta\tau = \Delta t/p$ inside the refined region with the second-order local time-stepping scheme (Algorithm 1). In the absence of local refinement, i.e. $p = 1$, the (local) time-stepping scheme corresponds to the standard leap-frog (LF) method and we denote by $\Delta t_{LF} = 0.5h^{\text{coarse}}$ (determined experimentally) the largest time-step allowed on that initial mesh. In the presence of local refinement, that is for $p \geq 2$, we denote by Δt_p the maximal time-step allowed. If $\Delta t_p = \Delta t_{LF}$, the local time-stepping scheme imposes no further restriction on Δt beyond that of the coarse mesh; then, we call the CFL condition of the scheme optimal.

To investigate the overall convergence rate, we consider a sequence of four successively refined regular meshes at fixed p, where in all instances $\Delta t_p = \Delta t_{LF}$ (the largest possible time-step for $p = 1$) – see Table 1. In Fig. 2, the L^2-error at time $T = 2\pi$ is shown versus the mesh size $h = h^{\text{coarse}}$. Independently of the number of local time-steps and the rate of local refinement $p = 1, 2, 4$ or 8, the numerical method yields overall second-order convergence for the optimal CFL condition. In Fig. 2, we also observe that the (discrete) energy $E^{n+1/2}$, defined in (28), is truly conserved for all time.

Next, we study the stability of the local time-stepping scheme. Recall that the scheme is stable if all eigenvalues of $(\Delta t^2/4)\mathbf{A}_p$ (see (27)) lie between zero and one; note that $\mathbf{A}_p$ also depends on Δt. Since the smallest eigenvalue always remains positive, it does not affect the stability here, which is fully determined by the maximal eigenvalue. In Fig. 3, we display the largest eigenvalue of $(\Delta t^2/4)\mathbf{A}_p$ for varying $\Delta t/\Delta t_{LF}$ for $p = 4$ and two different levels of (global) mesh refinement. We observe that for certain values of Δt, the maximal eigenvalue slightly transgresses the strict limit at one. However, as the mesh is refined the magnitude and the extent of the overshoot are reduced – compare the left and the right frame of Fig. 3 – and as a consequence do not affect the overall convergence of the scheme (on a fixed time interval). This somewhat subtle behavior, also observed for $p = 2$ and 8, is typical and always more prominent on regular meshes.

Table 1
Mesh data for each level of (global) refinement. The degree of local refinement is determined by p.

Level	p										
	1		2			4			8		
	el.	h	el.	h^{coarse}	h^{fine}	el.	h^{coarse}	h^{fine}	el.	h^{coarse}	h^{fine}
1	128	0.230	144	0.230	0.115	160	0.230	0.057	176	0.230	0.028
2	512	0.115	576	0.115	0.057	640	0.115	0.028	704	0.115	0.014
3	2048	0.057	2304	0.057	0.028	2,560	0.057	0.014	2,816	0.057	0.007
4	8192	0.028	9216	0.028	0.014	10,240	0.028	0.007	11,264	0.028	0.003

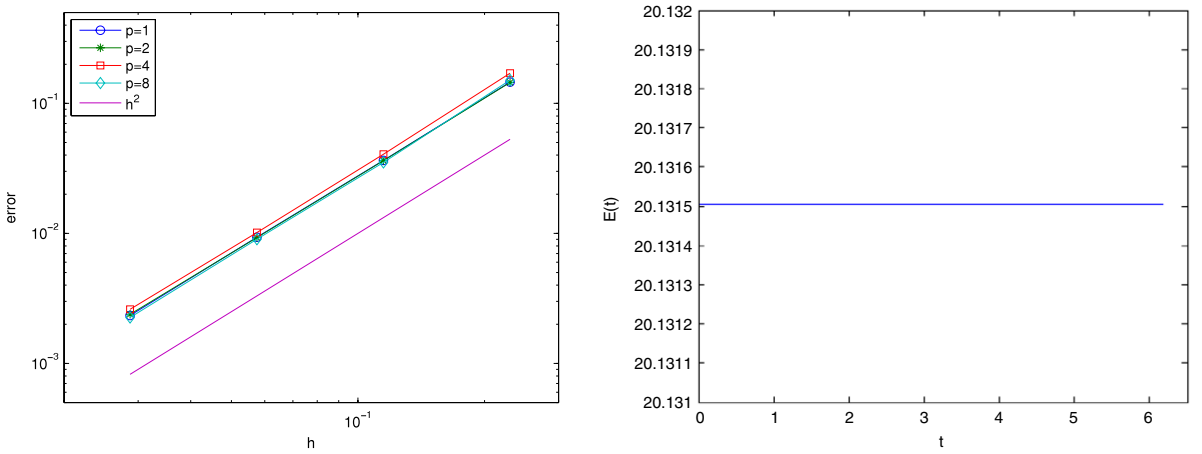

Fig. 2. L^2-error at time $T = 2\pi$ vs. $h = h^{\text{coarse}}$ (left). Time evolution of the discrete energy, defined in (28), with $p = 2$ and (global) refinement level 2 (right); note that the vertical scale is strongly magnified here.

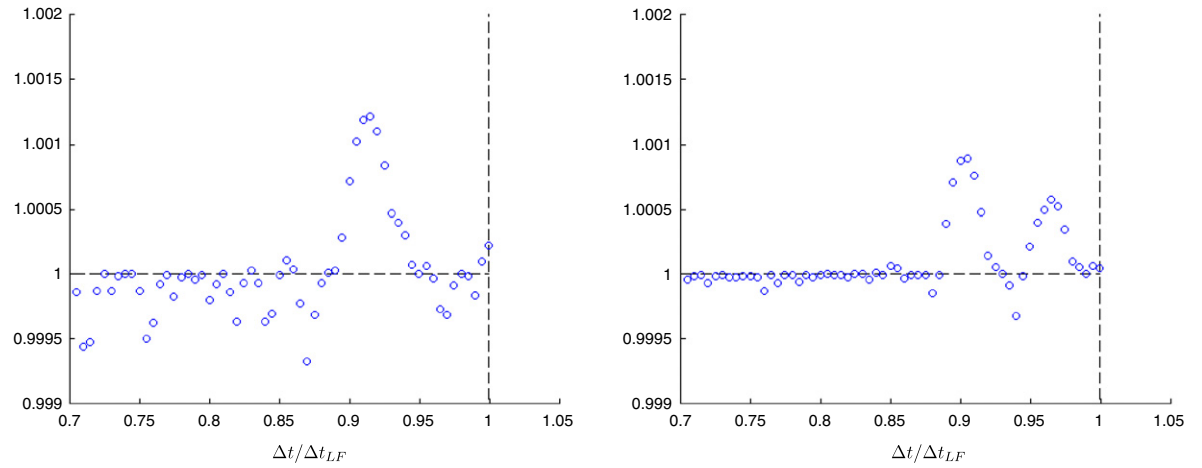

Fig. 3. The largest eigenvalues of $(\Delta t^2/4)\mathbf{A}_p$ for varying $\Delta t/\Delta t_{LF}$ with $p = 4$: (global) refinement level 1 (left), (global) refinement level 2 (right); the vertical scale is strongly magnified.

To illustrate this fact we now repeat the same experiment with an unstructured mesh, where again a small square subregion is refined by a factor $p = 4$, as shown in Fig. 4. Since the initial mesh in Ω is unstructured, the boundary between the fine and coarse mesh is not well-defined and we shall treat as fine mesh those triangles of size $h_K < 0.5h^{\text{coarse}}$. Again, for a sequence of successively refined meshes with $\Delta t_{LF} = 0.25h^{\text{coarse}}$ (determined experimentally), we obtain second-order convergence (not shown here). We now study the eigenvalues of $(\Delta t^2/4)\mathbf{A}_p$ for varying $\Delta t/\Delta t_{LF}$. As shown in the right frame of Fig. 4, the maximal eigenvalue still slightly transgresses the limit at one for certain values of Δt, yet the overshoot is much smaller here – compare with Fig. 3 – and occurs only at time steps $\Delta t > 0.9\Delta t_{LF}$. Thus, for all time-steps Δt smaller than $0.9\Delta t_{LF}$, the local time-stepping scheme is stable.

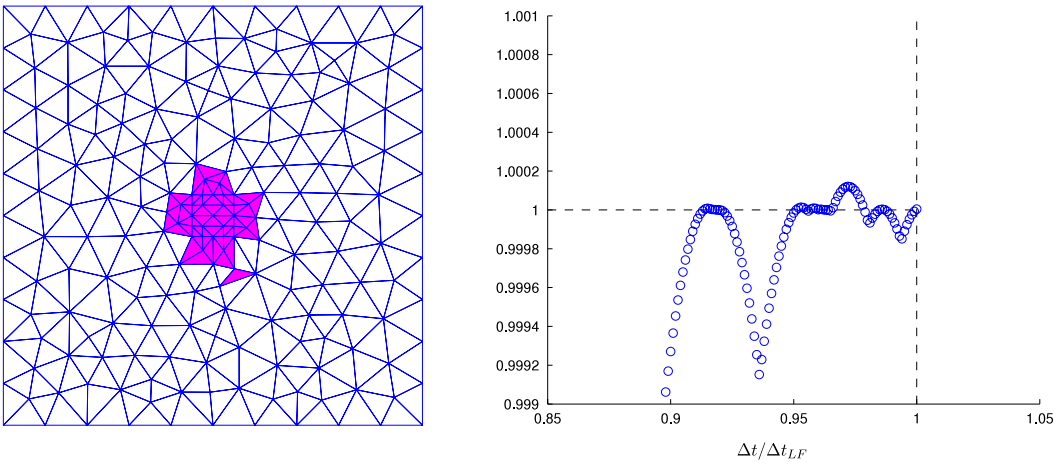

Fig. 4. The unstructured triangular mesh (left): 364 elements with $h^{\text{coarse}} = 0.067$ and $p = 4$; the darker triangles belong to the "fine" mesh and the lighter triangles to the "coarse" mesh. The largest eigenvalues of $(\Delta t^2/4)\mathbf{A}_p$ are shown for varying $\Delta t/\Delta t_{LF}$ on the unstructured mesh (right); here, the vertical scale is strongly magnified.

Table 2
Mesh data for each level of (global) refinement. The degree of local refinement is determined by p.

Level	p										
	1		2			4			8		
	el.	h	el.	h^{coarse}	h^{fine}	el.	h^{coarse}	h^{fine}	el.	h^{coarse}	h^{fine}
1	128	0.073	144	0.073	0.036	160	0.073	0.018	176	0.073	0.009
2	512	0.036	576	0.036	0.018	640	0.036	0.009	704	0.036	0.004
3	2048	0.018	2304	0.018	0.009	2,560	0.018	0.004	2,816	0.018	0.002
4	8192	0.009	9216	0.009	0.004	10,240	0.009	0.002	11,264	0.009	0.001

6.2. Inhomogeneous source inside conducting or non-conducting medium

Next, we consider the numerical solution of (1) in $\Omega = (-1, 1)^2$ until time $T = 0.5$, with constant material parameters $\varepsilon = \mu = 1$. We shall study two separate situations: an insulator with $\sigma = 0$ and a conductor with $\sigma = 1$. The initial and source data are chosen to match the smooth solution

$$\mathbf{u}(x, y, t) = \frac{t^2}{2}\begin{pmatrix} \cos(\pi x)\sin(\pi y) \\ -\sin(\pi x)\cos(\pi y) \end{pmatrix}.$$

Inside Ω, we choose a regular triangulation with $h^{\text{coarse}} = 0.073$. Then, we refine by a factor $p = 2$, 4 or 8 a square-shaped subregion of diagonal 0.5 at the centre of Ω. The fine mesh consists of triangles with size $h_K < h^{\text{coarse}}$. In Table 2, we present the mesh data of a sequence of four successively refined meshes. We always set the time-step to its (maximal) optimal value, $\Delta t_p = \Delta t_{LF} = 0.5h^{\text{coarse}}$ (determined experimentally with $p = 1$), and study the convergence of the two local time-stepping schemes: Algorithm 1 for $\sigma = 0$ and Algorithm 2 for $\sigma \neq 0$. In Fig. 5, we display the space–time L^2-errors of the numerical solutions at time $T = 0.5$ for different values of p. In all instances the numerical results corroborate the expected second-order rate of convergence.

6.3. Gaussian beam

Finally, we consider an electromagnetic wave propagating into a non-conducting square cavity $\Omega = (-1, 1)^2$, with a diamond-shaped hole of diagonal 0.2 at its centre – see Fig. 6. We set $\varepsilon = \mu = 1$ and let the initial conditions and the source term vanish throughout Ω. The electromagnetic field is excited at the top of Ω through the time-dependent inhomogeneous boundary condition

$$\mathbf{n} \times \mathbf{u}(x, y, t) = \begin{cases} g(x, t) & \text{at } y = 1, \quad -1 < x < 1, \\ 0 & \text{else,} \end{cases} \tag{49}$$

with

$$g(x, t) = \cos(2\pi t)\frac{1}{\sqrt{2\pi b}}\mathrm{e}^{\frac{-x^2}{2b^2}}, \quad b = 0.2.$$

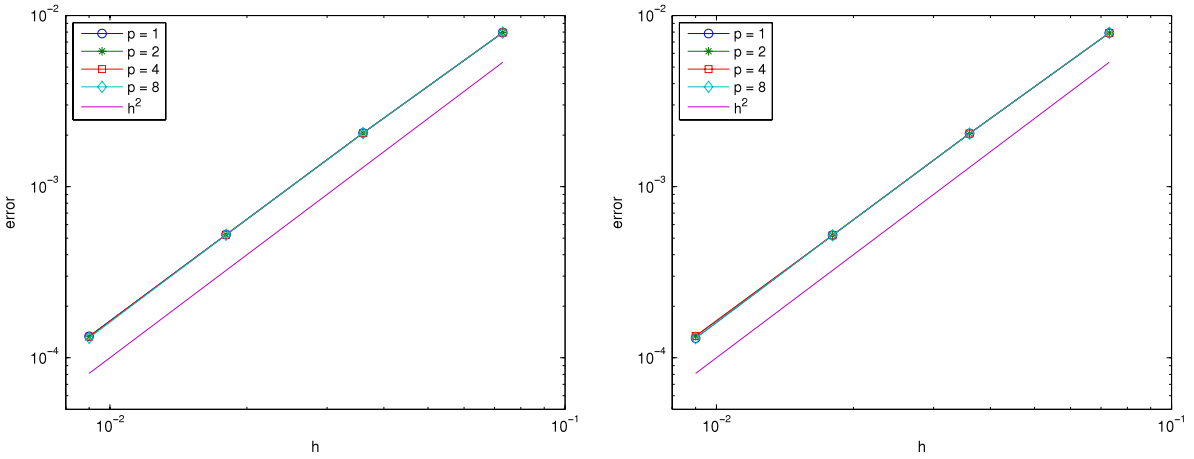

Fig. 5. L^2-error at time $T = 0.5$ vs. $h = h^{\text{coarse}}$: $\sigma = 0$ (left) and $\sigma = 1$ (right).

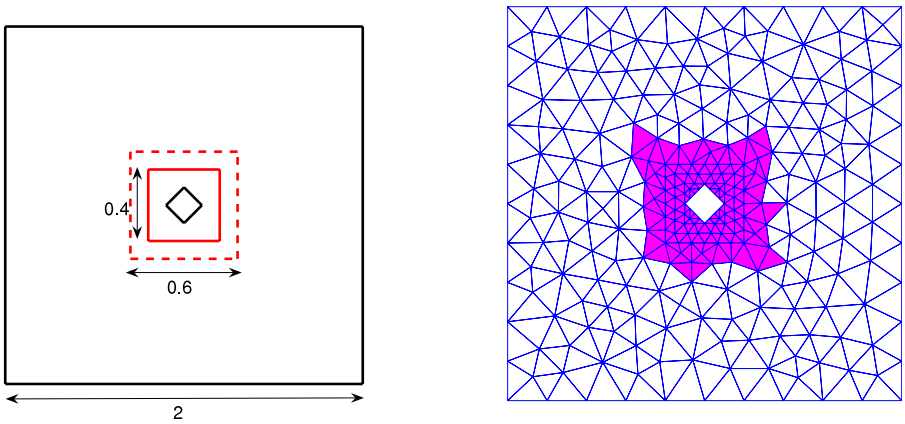

Fig. 6. The computational domain (left); the initial triangular mesh at (global) refinement level 1 (right): the darker triangles belong to the "fine" mesh.

The inhomogeneous boundary condition (49) is (weakly) imposed in the IP–DG discretisation by modifying (2) as follows: find $\mathbf{u}^h : [0, T] \to \mathbf{V}^h$ such that

$$(\mathbf{u}^h_{tt}, \mathbf{v}) + a_h(\mathbf{u}^h, \mathbf{v}) = (\mathbf{f}, \mathbf{v}) + \sum_{e \in \mathcal{E}_h^{\mathcal{B}}} \int_e g(\mathrm{a}(\mathbf{n} \times \mathbf{n}) - \nabla \times \mathbf{v})\, \mathrm{d}s, \quad \forall \mathbf{v} \in \mathbf{V}^h,\ t \in (0, T).$$

First, Ω is discretized with triangles of minimal size $h^{\text{coarse}} = 0.062$. Then, we refine the region $[-0.2, 0.2] \times [-0.2, 0.2]$ around the hole by a factor $p = 6$; hence, inside the locally refined region $h^{\text{fine}} = h^{\text{coarse}}/6$. Then, we successively refine the entire mesh four times, each time splitting every triangle into four. Again, since the initial mesh in Ω is unstructured, the boundary between the fine and coarse mesh is not well-defined and we shall treat as fine mesh those triangles, whose centre of gravity lies inside the box $[-0.3, 0.3] \times [-0.3, 0.3]$ – see Fig. 6. The corresponding degrees of freedom in the finite element solution are then selected merely by setting to one the corresponding diagonal entries of the matrix $\mathbf{P}$ in (10).

For the time discretisation we choose the local time-stepping method (Algorithm 1) from Section 4.1. Thus, the numerical method is second-order accurate in both space and time under the CFL condition $\Delta t = 0.19 h^{\text{coarse}}$, determined experimentally. If the same (global) time step Δt was used everywhere inside Ω, it would have to be about six times smaller than necessary in most of Ω. Instead, we use the local time-stepping method with $p = 6$, which for every time step Δt takes six local time steps inside the refined region.

In Fig. 7, the intensity of the electric field, $|\mathbf{u}| = \sqrt{u_1^2 + u_2^2}$ is shown at different times. The time-harmonic Gaussian beam, excited at the top of the computational domain Ω, propagates until it impinges on the hole. The resulting scattered circular wave then interferes with the incoming beam, as it reaches the lateral boundaries of Ω. Even stronger interferences occur as the beam is reflected back from the lower boundary, while singularities appear at the (re-entrant) corners of the hole.

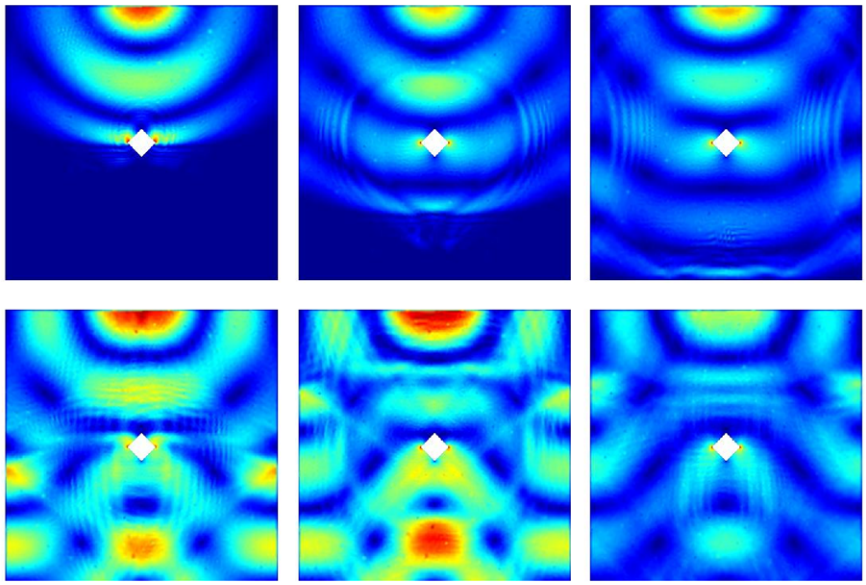

Fig. 7. Gaussian beam penetrating a cavity with a small diamond-shaped hole from above. The intensity of the electric field, $|\mathbf{u}| = \sqrt{u_1^2 + u_2^2}$, at times $t = 1, 1.5, 2, 3, 3.5$ and 4.5.

7. Conclusion

Starting from the standard second-order leap-frog scheme, we have presented explicit local time-stepping methods for Maxwell's equations, which allow arbitrarily small time-steps precisely where the smallest elements in the mesh are located. When combined with a finite element discretisation in space with an essentially diagonal mass matrix, the resulting discrete time-marching schemes are fully explicit. The second-order accurate schemes are given by Algorithm 1 (Section 4.1) and Algorithm 2 (Section 4.2) in a non-conducting or conducting medium, respectively. A fourth-order accurate scheme is given by Algorithm 3 (Section 5) for a non-conducting media, while higher order extensions are straightforward. In a source-free and non-conducting medium, these local time-stepping schemes also conserve (a discrete version of the) energy, which not only provides a rigorous criterion for numerical stability but also is of practical importance for long-time simulations. In a conducting medium, the stability of the local time-stepping scheme remains independent of the magnitude of the conductivity.

Since the local time-stepping methods presented here are truly explicit, their parallel implementation is straightforward. Let Δt denote the time-step imposed by the CFL condition in the coarser part of the mesh. Then, during every (global) time-step Δt, each local time-step of size $\Delta t/p$ inside the fine region of the mesh, simply corresponds to sparse matrix–vector multiplications that only involve the degrees of freedom associated with the fine region of the mesh. Those "fine" degrees of freedom can be selected individually and without any restriction by setting the corresponding entries in the diagonal projection matrix P to one; in particular, no adjacency or coherence in the numbering of the degrees of freedom is assumed. Hence the implementation is straightforward and requires no special data structures. In the presence of multi-level mesh refinement, each local time-step in the fine region can itself include further local time-steps inside a smaller subregion with an even higher degree of local mesh refinement.

Acknowledgements

We thank David Cohen for useful comments and suggestions.

References

[1] K.S. Yee, Numerical solution of initial boundary value problems involving Maxwell's equations in isotropic media, IEEE Trans. Antennas Propag. 14 (1966) 302–307.
[2] A. Taflove, Computational Electrodynamics: The Finite-Difference Time-Domain Method, Artech House, Boston, 1995.
[3] J.C. Nédélec, Mixed finite elements in $\mathbb{R}^3$, Numer. Math. 35 (1980) 315–341.
[4] J.C. Nédélec, A new family of mixed finite elements in $\mathbb{R}^3$, Numer. Math. 50 (1986) 57–81.
[5] G. Rodrigue, D. White, A vector finite element time-domain method for solving Maxwell's Equations on unstructured hexahedral grids, SIAM J. Sci. Comput. 23 (2001) 683–701.
[6] R.L. Lee, N.K. Madsen, A mixed finite element formulation for Maxwell's equations in the time domain, J. Comput. Phys. 88 (1990) 284–304.
[7] K.D. Paulsen, D.R. Lynch, Elimination of vector parasites in finite element Maxwell solutions, IEEE Trans. Microwave Theory Tech. 39 (1991) 395–404.
[8] P. Monk, Finite Element Methods for Maxwell's Equations, OUP, New York, 2003.

[9] A. Elmkies, P. Joly, Finite elements and mass lumping for Maxwell's equations: the 2D case, C. R. Acad. Sci. Paris 324 (1997) 1287–1293.
[10] B. Cockburn, C.-W. Shu, TVB Runge–Kutta local projection discontinuous Galerkin method for conservation laws II: general framework, Math. Comp. 52 (1989) 411–435.
[11] M.-H. Chen, B. Cockburn, F. Reitich, High-order RKDG methods for computational electromagnetics, J. Sci. Comput. 22 (2005) 205–226.
[12] T. Warburton, Application of the discontinuous Galerkin method to Maxwell's equations using unstructured polymorphic *hp*-finite elements, in: B. Cockburn, G.E. Karniadakis, C.-W. Shu (Eds.), Discontinuous Galerkin Methods: Theory, Computation and Applications, in: Lecture Notes in Computer Science Engineering, vol. 11, Springer, Berlin, 2000, pp. 451–458.
[13] J.S. Hesthaven, T. Warburton, Nodal high-order methods on unstructured grids I: time-domain solution of Maxwell's equations, J. Comp. Phys. 181 (2002) 186–221.
[14] D. Sármány, M.A. Botchev, J.J.W. van der Vegt, Dispersion and dissipation error in high-order Runge–Kutta discontinuous Galerkin discretisations of the Maxwell equations, J. Sci. Comput. 33 (2007) 47–74.
[15] M.J. Grote, A. Schneebeli, D. Schötzau, Interior penalty discontinuous Galerkin method for Maxwell's equations: energy norm error estimates, J. Comput. Appl. Math. 204 (2007) 375–386.
[16] M.J. Grote, A. Schneebeli, D. Schötzau, Interior penalty discontinuous Galerkin method for Maxwell's equations: optimal l^2-norm error estimates, IMA J. Numer. Anal. 28 (2008) 440–468.
[17] M.J. Grote, D. Schötzau, Optimal error estimates for the fully discrete interior penalty DG method for the wave equation, J. Sci. Comput. 40 (2009) 257–272.
[18] F. Collino, T. Fouquet, P. Joly, A conservative space–time mesh refinement method for the 1-D wave equation. I. construction, Numer. Math. 95 (2003) 197–221.
[19] J.G. Verwer, Convergence and component splitting for the Crank–Nicolson–Leap–Frog integration method, CWI Tech. Report MAS-E0902, 2009.
[20] F. Collino, T. Fouquet, P. Joly, Conservative space–time mesh refinement method for the FDTD solution of Maxwell's equations, J. Comput. Phys. 211 (2006) 9–35.
[21] J.S. Hesthaven, T. Warburton, Nodal Discontinuous Galerkin Methods, Springer, 2008.
[22] S. Piperno, Symplectic local time-stepping in non-dissipative DGTD methods applied to wave propagation problems, M2AN Math. Model. Numer. Anal. 40 (2006) 815–841.
[23] E. Montseny, S. Pernet, X. Ferriéres, G. Cohen, Dissipative terms and local time-stepping improvements in a spatial high order discontinuous Galerkin scheme for the time-domain Maxwell's equations, J. Comput. Phys. 227 (2008) 6795–6820.
[24] A. Buffa, I. Perugia, Discontinuous Galerkin approximation of the Maxwell eigenproblem, SIAM J. Numer. Anal. 44 (2006) 2198–2226.
[25] J. Diaz, M.J. Grote, Energy conserving explicit local time-stepping for second-order wave equations, SIAM J. Sci. Comput. 31 (2009) 1985–2014.
[26] A. Taube, M. Dumbser, C.-D. Munz, R. Schneider, A high-order discontinuous Galerkin method with time-accurate local time stepping for the Maxwell equations, Int. J. Numer. Model. 22 (2009) 77–103.
[27] J.L. Lions, E. Magenes, Non-Homogeneous Boundary Value Problems and Applications, vol. I, Springer, 1972.
[28] A. Buffa, I. Perugia, T. Warburton, The mortar-discontinuous galerkin method for the 2D Maxwell eigenproblem, J. Sci. Comp. 40 (2009) 86–114.
[29] D.N. Arnold, F. Brezzi, B. Cockburn, L.D. Marini, Unified analysis of discontinuous Galerkin methods for elliptic problems, SIAM J. Numer. Anal. 39 (2001) 1749–1779.
[30] P. Houston, I. Perugia, D. Schötzau, Mixed discontinuous Galerkin approximation of the Maxwell operator, SIAM J. Numer. Anal. 42 (2004) 434–459.
[31] E. Hairer, C. Lubich, G. Wanner, Geometric Numerical Integration, Structure-Preserving Algorithms for Ordinary Differential Equations, Springer, 2002.
[32] R. Rieben, D. White, G. Rodrigue, High-order symplectic integration methods for finite element solutions to time dependent Maxwell equations, IEEE Trans. Antennas Propagat. 52 (2004) 2190–2195.
[33] G.R. Shubin, J.B. Bell, A modified equation approach to constructing fourth order methods for acoustic wave propagation, SIAM J. Sci. Stat. Comput. 8 (1987) 135–151.
[34] M.A. Botchev, J.G. Verwer, Numerical integration of damped Maxwell equations, SIAM J. Sci. Comput. 31 (2009) 1322–1346.
[35] G. Cohen, P. Joly, J.E. Roberts, N. Tordjman, Higher order triangular finite elements with mass lumping for the wave equation, SIAM J. Numer. Anal. 38 (2001) 2047–2078.